A simplified Kirchhoff-Love large deformation model for elastic shells and its effective isogeometric formulation

Leonardo Leonetti[a,*], Domenico Magisano[a], Antonio Madeo[a], Giovanni Garcea[a], Josef Kiendl[b], Alessandro Reali[c]

[a] *Dipartimento di Ingegneria Informatica, Modellistica, Elettronica e Sistemistica, Università della Calabria, Italy*
[b] *Department of Marine Technology, Norwegian University of Science and Technology, Norway*
[c] *Department of Civil Engineering and Architecture, University of Pavia, Italy*

Abstract

Isogeometric Kirchhoff-Love elements have received an increasing attention in geometrically nonlinear analysis of elastic shells. Nevertheless, some difficulties still remain. Among the others, the highly nonlinear expression of the strain measure, which leads to a complicated and costly computation of the discrete operators, and the existence of locking, which prevents the use of coarse meshes for slender shells and low order NURBS, are key issues that need to be addressed. In this work, exploiting the hypothesis of small membrane strains, we propose a simplified strain measure with a third order polynomial dependence on the displacement variables which allows an efficient evaluation of the discrete quantities. Numerical results show practically no difference to the original model, even for very large displacements and composite structures. Patch-wise reduced integrations are then investigated to deal with membrane locking in large deformation problems. An optimal integration scheme for third order C^2 NURBS, in terms of accuracy and efficiency, is identified. Finally, the recently proposed Newton method with mixed integration points is used for the solution of the discrete nonlinear equations with a great reduction of the iterative burden with respect to the standard Newton scheme.

Keywords: Geometric nonlinearities, isogeometric analysis, Kirchhoff-Love shells, composites, reduced integration, MIP Newton

1. Introduction

Shell structures are commonly employed in a wide range of engineering applications. When the thickness is significantly smaller compared to the other dimensions, these structures exhibit large deformations while the material behaves elastically. Different structural models can be used to simulate the mechanical behavior of shells. The most common ones are those based on the Mindlin-Reissner hypotheses and the Kirchhoff-Love ones. In the first case, the kinematics is governed by displacements and rotations of the middle surface, while in the second one only displacements are needed.

Although the Kirchhoff-Love model well describes the behavior of thin shells, it has not been widely used in the past due to the C^1 continuity required by the weak formulation, not easily obtainable in standard finite element models. The Mindlin-Reissner model has been then often preferred also when the Kirchhoff-Love hypotheses are likely to be verified. The main difficulty in using Mindlin-Reissner shells in large deformation problems is the need of handling finite rotations, which leads to very long, complicated and expensive formulas. For this reason, alternative formulations have been investigated, like solid-shells, which

*Corresponding author
Email addresses: leonardo.leonetti@hotmail.it (Leonardo Leonetti), domenico.magisano@unical.it (Domenico Magisano), antonio.madeo81@unical.it (Antonio Madeo), giovanni.garcea@unical.it (Giovanni Garcea), josef.kiendl@ntnu.no (Josef Kiendl), alessandro.reali@unipv.it (Alessandro Reali)

are solids able to obtain the shell solution with just one element through the thickness. Based on a solid model, such formulations use displacement degrees of freedom (DOFs) only. The number of overall DOFs in solid-shell elements can be equal to the one in Mindlin-Reissner elements [1, 2].

Isogeometric analysis (IGA) [3, 4] opened new attractive possibilities for the use of the Kirchhoff-Love model. IGA is based on splines (like, e.g., B-splines or NURBS), interpolation functions which make it possible to fulfill the continuity requirement easily. This kind of analysis spread rapidly in the scientific community for a wide range of mechanical problems. Among the main reasons for its success is, in our opinion, the way it makes it possible to elevate order and continuity of the basis functions while practically maintaining the same number of DOFs of linear Lagrangian interpolations. Another notable feature is that the high continuity of the shape functions allows the total number of integration points to be reduced significantly as shown in [5–8]. Finally, the geometry of shells is reproduced exactly, regardless of the mesh adopted, and a simple link between CAD and structural analysis is available. These considerations make IGA very attractive, particularly in geometrically nonlinear analysis where a highly continuous solution is often expected, like for instance in buckling problems [9, 10]. Some examples of isogeometric Mindlin-Reissner formulations can be found in [6, 11–14], while solid-shell implementations are proposed in [2, 15–17]. For the Kirchhoff-Love model, we refer to [18–22]. A recent work [23] proposed a shear deformable isogeometric shell model without explicitly using rotation variables. We would also like to mention the use of B-spline functions for Kirchhoff plates [24, 25] as well as the use of C^1-comforming subdivision surfaces for Kirchhoff-Love shells [26] prior to the seminal work of Hughes on IGA.

The Kirchhoff-Love model is potentially able to furnish the most efficient analysis, due to the reduced number of DOFs. However, the cost to pay for this advantage is a more complicated strain measure, compared to solid-shell models, and a consequent effort for the derivation and the computation of the discrete quantities. As opposite to the other options, the Kirchhoff-Love model a priori avoids shear locking. However, like all the other ones, it is affected by membrane locking for curved shells already in the linear range when the standard displacement-based formulation is employed. Moreover, locking occurs, even for initially flat plates, when the displacements get large, due the different approximation of the linear and the nonlinear part of the membrane strains. Increasing the order of the shape functions reduces the locking but, at the same time, increases the computational burden for the assembly of the discrete operators and for the solution of the discrete equations because of the decreasing stiffness matrix sparsity. For these reasons, second order C^1 and third order C^2 NURBS are often preferred, even if they are not immune to locking. Due to the inter-element high continuity of the interpolation, element-wise reduced integrations and strategies, like ANS [15], only alleviate, but do not eliminate locking, and may not be sufficiently effective for very thin shells. The same consideration holds for mixed formulations with stress shape functions defined at the element level. Limited to the linear elastic case, an alternative local $\bar{B}$ formulation has been proposed in [27]. Conversely, mixed formulations with continuous stress shape functions have been successfully proposed [12, 17, 28] to eliminate locking in linear and nonlinear problems. In [13] a variational formulation based on two kinematic fields is proposed to achieve locking-free solutions without the need of choosing the stress interpolation. In both these last two cases, the number of variables involved in the global operations increases with respect to the standard displacement formulation. The static condensation of the extra variables, usually employed in FE analysis and performed at the element level, can be carried out only at patch level and is not convenient because it results in a fully populated condensed stiffness matrix. An interesting alternative is the use of displacement formulations with patch-wise reduced integration rules [5]. They have been initially proposed to alleviate and, in some cases, eliminate locking in geometrically linear analysis of two-dimensional elasticity and Reissner–Mindlin shell problems [6]. A significantly lower number of integration points is employed compared to the Gauss quadrature, so improving also the computational efficiency. This strategy seems more attractive than a mixed formulation, since it preserves the stiffness matrix sparsity without introducing additional unknowns and allows a more efficient integration. This strategy has been recently applied to solid-shell models in geometrically nonlinear problems [2, 29]. This study shows excellent results for third order C^2 NURBS, while the results obtained for the second order C^1 case are generally not as good as in linear elastic problems [6]. So far, no study is available to our knowledge concerning optimal patch-wise reduced integrations for the geometrically nonlinear Kirchhoff-Love shell model.

Compared to Mindlin-Reissner and solid-shell models, the Kirchhoff-Love one makes the modeling of boundary conditions and coupling patches not trivial. However, an intensive research has been carried out in recent years [30–33] which led to practical solutions.

When comparing mixed and displacement formulations in path-following methods for geometrically nonlinear analyses, many authors observed a more robust and efficient iterative solution for mixed formulations. The reason for this is explained in [34, 35] where it is shown that the performance of Newton's method drastically deteriorates in displacement formulations when the slenderness of a structure gets higher. To eliminate this inconvenience in displacement-based finite elements, the Mixed Integration Point (MIP) strategy has been recently proposed in [36]. It consists of a relaxation of the constitutive equations at each integration point during the Newton iterative process. The MIP Newton's method can withstand much larger step sizes (increments) with a reduced number of iterations to obtain an equilibrium point compared to a standard Newton's strategy. It received particular attention in displacement-based IGA for its simplicity and effectiveness. In particular, it was firstly used in the IGA context in [2] for a solid-shell model in weak form, while it was applied to Kirchhoff rods in [37] and [38], which provides also a successful extension to the strong form.

In this work, we propose an isogeometric Kirchhoff-Love formulation for the geometrically nonlinear analysis of homogeneous and multi-layered composite shells. In order to reduce the computational burden for the discrete operators, the standard strain measure is simplified exploiting the hypothesis of small membrane strains. The obtained model is characterized by a strain measure with a simple third order dependence on the displacement DOFs, which leads to a simpler and compact expression of the discrete quantities and reduces the computational effort for the evaluation of the discrete operators. A strategy based on patch-wise reduced integration rules, previously assessed for a large deformation solid-shell model, is investigated in the proposed Kirchhoff-Love shell model with the aim of avoiding locking when second order C^1 and third order C^2 NURBS are adopted while increasing computational efficiency. In particular, an optimal integration scheme for third order C^2 NURBS, in terms of both accuracy and efficiency, is identified. The obtained displacement-based formulation seems able to provide accurate solutions, practically unaffected by locking, avoiding the need of a mixed formulation and the corresponding, previously discussed, drawback. The recently introduced MIP Newton method is used for the solution of the nonlinear discrete equations for reducing the iterative burden.

The paper is organized as follows: section 2 presents the isogeometric Kirchhoff-Love shell model for large deformations and derives the simplified strain measure based on the hypothesis of small membrane strains; in section 3 patch-wise reduced integrations are investigated to deal with interpolation locking in the nonlinear range; numerical tests are carried out in section 4 to validate both the accuracy of the proposed shell model and the effectiveness of a patch-wise reduced integration in avoiding locking; finally conclusions are drawn in section 5.

2. The isogeometric Kirchhoff-Love shell model: standard and simplified version

In this section the isogeometric Kirchhoff-Love model for geometrically nonlinear analysis of shells is presented. After a very brief introduction to the NURBS basics, the standard Kirchhoff-Love model is recalled (see [18] for further details). The strain measure of such a model and its derivatives are complicated nonlinear functions of the displacement DOFs and lead to a difficult and costly evaluation of the discrete operators, which consist of very long expressions. The hypothesis of small membrane strains is exploited to derive a novel simplified strain measure, which is just a third order polynomial function. Both homogeneous and multi-layered shells are considered. In this second case, the homogenized material law of the shell is obtained from the elastic properties of each orthotropic lamina, taking into account the fiber orientation.

2.1. NURBS basics

A B-Spline curve is represented as

$$\mathbf{u}(\xi) = \sum_{i=1}^{n} N_i^p(\xi)\mathbf{P}_i = \mathbf{N}(\xi)\mathbf{P} \tag{1}$$

where $\mathbf{P}_i$, $i = 1 \cdots n$ are the control points and $N_i^p(\xi)$ are the set of B-Spline basis functions, which are piecewise polynomial functions of order p. The latter are defined by a set of non-decreasing real numbers $\Xi = [\xi_1, \xi_2, ..., \xi_{n+p+1}]$ known as knot vector. More details on the B-Spline parametrization can be found in [39]. B-spline basis functions are calculated recursively by using the formula

$$N_i^p(\xi) = \frac{\xi - \xi_i}{\xi_{i+p} - \xi_i} N_i^{p-1}(\xi) + \frac{\xi_{i+p+1} - \xi}{\xi_{i+p+1} - \xi_{i+1}} N_{i+1}^{p-1}(\xi)$$

for $p \geq 1$ and starting from piecewise constant functions ($p = 0$) defined as

$$N_i^0(\xi) = \begin{cases} 1, & \text{if} \quad \xi_i \leq \xi < \xi_{i+1} \\ 0, & \text{otherwise.} \end{cases}$$

B-Spline basis functions have attractive properties: they satisfy the partition of unity that makes them suitable for discretization methods, have a compact support and are non-zero and non-negative within the knot interval $[\xi_i, \xi_{i+p+1}]$. The regularity r between two parametric or physical elements is described by the multiplicity of the associated knot in Ξ. The regularity is given by $r = p - s$ where p and s are the order used for the basis functions and the multiplicity of the knot ξ_i respectively.

Since B-splines are piece-wise polynomial functions they are not able to represent circular arcs and conic sections exactly. For this reason, NURBS have been introduced extending the B-spline concept to represent these objects exactly. NURBS are obtained by a projective transformation of B-splines extending Eq.(1) by using as shape functions

$$R_i^p(\xi) = \frac{N_i^p(\xi) w_i}{\sum_{k=1}^n N_k^p(\xi) w_k} \tag{2}$$

where w_i are the so-called weights. It is worth noting that all properties of B-Splines are maintained and, in particular, B-Splines are retrieved when all the weights are equal.

By applying the tensor product, a NURBS surface is constructed in a similar way to Eq.(1) as

$$\mathbf{u}(\xi, \eta) = \sum_{i=1}^{n} \sum_{j=1}^{m} R_i^p(\xi) M_j^q(\eta) \mathbf{P}_{ij} = \mathbf{N}(\xi, \eta) \mathbf{P} \tag{3}$$

where $\Xi = [\xi_1, \xi_2 ... \xi_{n+p+1}]$ and $\mathcal{H} = [\eta_1, \eta_2 ... \eta_{m+q+1}]$ are two knot vectors, R_i^p and M_j^q are the one-dimensional basis functions over these knot vectors and $\mathbf{P}_{ij}$ defines a set of $n \times m$ control points. The tensor product of the knot vectors Ξ and $\mathcal{H}$ defines a mesh of quadrilateral "isogeometric elements".

In this paper we deal only with NURBS with maximum regularity, that is $r = p - 1$. For this reason, in the following sections the label C^1 is used to denote NURBS with $p = 2$ and $r = 1$, while C^2 means $p = 3$ and $r = 2$.

2.2. Kirchhoff–Love shell kinematics

We use a Total Lagrangian formulation to identify material points on the middle surface of the current configuration in terms of their position vector $\mathbf{X}(\xi, \eta)$ in the reference configuration and the displacement field $\mathbf{u}(\xi, \eta)$

$$\mathbf{x}(\xi, \eta) = \mathbf{X}(\xi, \eta) + \mathbf{u}(\xi, \eta) \tag{4}$$

where $\boldsymbol{\xi} = [\xi, \eta]$ denotes convective curvilinear shell coordinates with (ξ, η) representing in-plane coordinates (cf. Fig. 1). The middle surface covariant basis vectors in the undeformed and deformed configuration are obtained from the corresponding partial derivatives of the position vectors $\mathbf{X}$ and $\mathbf{x}$, respectively

$$\mathbf{G}_i = \mathbf{X}_{,i} \,, \qquad \boldsymbol{g}_i = \mathbf{x}_{,i} = \mathbf{G}_i + \mathbf{u}_{,i} \qquad \text{with} \;\; i = 1, 2 \,, \tag{5}$$

where $()_{,i}$ denotes the partial derivative with respect to the i-th component of $\boldsymbol{\xi}$, while the unit normal ones are

$$\mathbf{G}_3 = \frac{\mathbf{G}_1 \times \mathbf{G}_2}{\|\mathbf{G}_1 \times \mathbf{G}_2\|} \quad , \quad \boldsymbol{g}_3 = \frac{\boldsymbol{g}_1 \times \boldsymbol{g}_2}{\|\boldsymbol{g}_1 \times \boldsymbol{g}_2\|} \tag{6}$$

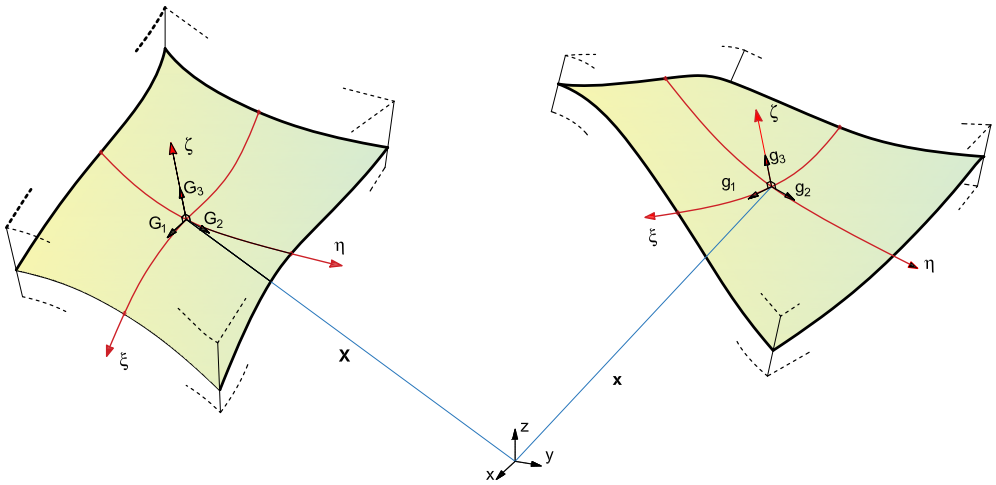

Figure 1: Undeformed and deformed shell geometry.

which corresponds to the Kirchhoff-Love (KL) shell assumption that the director remains straight and normal to the mid-surface during deformation.

The contravariant basis vectors follow from the dual basis condition: $\boldsymbol{g}_i \cdot \boldsymbol{g}^j = \mathbf{G}_i \cdot \mathbf{G}^j = \delta_i^j$ and the metric coefficients are $g_{ij} = \boldsymbol{g}_i \cdot \boldsymbol{g}_j$ and $G_{ij} = \mathbf{G}_i \cdot \mathbf{G}_j$ with $i, j = 1, 2$.

The curvature tensor coefficients are defined as in [18]

$$B_{ij} = -\frac{1}{2}\left(\mathbf{G}_i \cdot \mathbf{G}_{3,j} + \mathbf{G}_j \cdot \mathbf{G}_{3,i}\right) = \mathbf{G}_{i,j} \cdot \mathbf{G}_3,$$
$$b_{ij} = -\frac{1}{2}\left(\boldsymbol{g}_i \cdot \boldsymbol{g}_{3,j} + \boldsymbol{g}_j \cdot \boldsymbol{g}_{3,i}\right) = \boldsymbol{g}_{i,j} \cdot \boldsymbol{g}_3.$$

The motion of material points from the initial reference configuration to the current configuration is described by the deformation gradient $\mathbf{F}$

$$\mathbf{F} = \boldsymbol{g}_i \otimes \mathbf{G}^i. \tag{7}$$

Einstein's convention of summing on repeated indexes is adopted from now on.
Using the deformation gradient in Eq.(7) and the metric tensor coefficients g_{ij} and G_{ij}, the Green-Lagrange strain tensor reduces to

$$\mathbf{E} = \bar{E}_{ij}\, \mathbf{G}^i \otimes \mathbf{G}^j \quad i, j = 1, 2 \tag{8}$$

where $\bar{E}_{ij}$ are the covariant strain components. Due to Eq.(6) the transverse shear strains vanish, that is $E_{i3} = 0, i = 1, 2$. Assuming the strain to vary linearly through the thickness, it is possible to separate the strain into a constant part due to membrane action and a linear part due to bending. The covariant strain coefficients are

$$\bar{E}_{ij} = \bar{e}_{ij} + \zeta \bar{\chi}_{ij} = \frac{1}{2}\left(g_{ij} - G_{ij}\right) + \zeta(B_{ij} - b_{ij}) \quad \text{with} \quad i, j = 1, 2 \tag{9}$$

with $\zeta \in [-t/2, t/2]$ and t the thickness of the shell.

2.3. A consistent approximation of curvature

The curvature for a Kirchhoff-Love shell is

$$\bar{\chi}_{ij} = B_{ij} - b_{ij} = \left(\mathbf{G}_{i,j} \cdot \mathbf{G}_3 - \boldsymbol{g}_{i,j} \cdot \boldsymbol{g}_3\right) \quad i, j = 1, 2$$

with

$$\boldsymbol{g}_3 = \frac{\boldsymbol{g}_1 \times \boldsymbol{g}_2}{\|\boldsymbol{g}_1 \times \boldsymbol{g}_2\|} \quad \boldsymbol{g}_i = \mathbf{F}\mathbf{G}_i \; i = 1, 2$$

The presence of the norm $\|\boldsymbol{g}_1 \times \boldsymbol{g}_2\|$ leads to a complicated curvature expression in terms of the displacement DOFs and then to a significant computational effort for the evaluation of the discrete quantities. In this work, we propose an alternative strain measure, which exploits the hypothesis of large deformations but small membrane strains. This idea was initially proposed in [40] for flat plates and is here extended to general shells.

We can note that $\|\boldsymbol{g}_1 \times \boldsymbol{g}_2\|$ represents the area of the parallelogram having $\boldsymbol{g}_1$ and $\boldsymbol{g}_2$ as sides.

The polar decomposition of the deformation gradient states that $\mathbf{F} = \mathbf{RU}$, with $\mathbf{R}$ the rotation tensor and $\mathbf{U}$ the stretch tensor. Using simple properties of the cross product, we have

$$\boldsymbol{g}_1 \times \boldsymbol{g}_2 = \mathbf{R}\{(\mathbf{U}\mathbf{G}_1) \times (\mathbf{U}\mathbf{G}_2)\}$$

and then

$$\|\boldsymbol{g}_1 \times \boldsymbol{g}_2\| = \|(\mathbf{U}\mathbf{G}_1) \times (\mathbf{U}\mathbf{G}_2)\| \tag{10}$$

Exploiting the small membrane strain hypothesis, while the rotation $\mathbf{R}$ is arbitrary large, we have $\mathbf{U}\mathbf{G}_1 \approx \mathbf{G}_1$ and $\mathbf{U}\mathbf{G}_2 \approx \mathbf{G}_2$. In this case we obtain the following simplification

$$\|\boldsymbol{g}_1 \times \boldsymbol{g}_2\| \approx \|\mathbf{G}_1 \times \mathbf{G}_2\|$$

that means that the parallelogram area before and after deformation is almost the same, while the direction of the normal vector can undergo arbitrarily large rotations.

Consequently, b_{ij} is redefined as

$$b_{ij}^{SKL} = \boldsymbol{g}_{i,j} \cdot \frac{\boldsymbol{g}_1 \times \boldsymbol{g}_2}{\|\mathbf{G}_1 \times \mathbf{G}_2\|}.$$

and the curvature simplifies to

$$\bar{\chi}_{ij} = B_{ij} - b_{ij}^{SKL} = \frac{1}{\|\mathbf{G}_1 \times \mathbf{G}_2\|}\left(\mathbf{G}_{i,j} \cdot (\mathbf{G}_1 \times \mathbf{G}_2) - \boldsymbol{g}_{i,j} \cdot (\boldsymbol{g}_1 \times \boldsymbol{g}_2)\right) \quad i,j = 1,2 \tag{11}$$

The model so obtained will be called *simplified* Kirchhoff-Love (SKL) from now on.

2.3.1. Error estimate

Although the simplified curvature of the SKL model allows for simple and low cost expressions of the discrete operators, one can be interested in having a quantitative estimate of the error compared to the exact KL model. To this end, let us introduce the Biot strain tensor at the middle surface of the shell $\mathbf{E}_b \equiv \mathbf{U} - \mathbf{I}$. By choosing a local Cartesian system $\boldsymbol{i}_1, \boldsymbol{i}_2$ lying on the middle surface of the shell, $\mathbf{E}_b$, $\mathbf{G}_1$ and $\mathbf{G}_2$ can be expressed as

$$\mathbf{E}_b = E_{bij}\boldsymbol{i}_i \otimes \boldsymbol{i}_j, \quad \mathbf{G}_1 = G_{1i}\boldsymbol{i}_i, \quad \mathbf{G}_2 = G_{2i}\boldsymbol{i}_i, \quad i,j = 1,2.$$

By evaluating Eq.(10) with $\mathbf{U} = \mathbf{I} + \mathbf{E}_b$, we obtain

$$\|\boldsymbol{g}_1 \times \boldsymbol{g}_2\| = \|\mathbf{G}_1 \times \mathbf{G}_2\|(1+\alpha) \quad \text{with} \quad \alpha = E_{b11} + E_{b22} + E_{b11}E_{b22} - E_{b12}^2 > -1$$

and then

$$\frac{|b_{ij} - b_{ij}^{SKL}|}{|b_{ij}|} = |\alpha|.$$

For most structural materials, in order to work in the elastic range, $|\alpha|$ is limited to values of the order of 10^{-3} and then so is the maximum error expected on the curvature. In typical shell problems, the membrane stiffness tends to infinity compared to the flexural one. This implies values of $|\alpha|$ much lower than the elastic limit. For these reasons, differences between the original and the simplified model are not easily spotted in practical computations when working in the small strain range.

2.4. The isogeometric shell element

Following the isogeometric concept, geometry and displacement fields are interpolated, over the element, as follows

$$\mathbf{X}(\xi,\eta)=\mathbf{N}_u(\xi,\eta)\mathbf{X}_e,\quad \mathbf{u}(\xi,\eta)=\mathbf{N}_u(\xi,\eta)\mathbf{d}_e \tag{12}$$

where $\mathbf{X}_e$ and $\mathbf{d}_e$ collect the element control points and the element control displacements, respectively. The matrix $\mathbf{N}_u(\xi,\eta)$ collects bivariate NURBS functions [3].

Adopting Voigt's notation, the covariant strain components in Eq.(9) are collected in the vector $\bar{\mathbf{E}}=[\bar{E}_{\xi\xi},\bar{E}_{\eta\eta},2\bar{E}_{\xi\eta}]^T$, that, exploiting Eq.(12), becomes

$$\bar{\mathbf{E}}=\bar{\mathbf{e}}+\zeta\bar{\boldsymbol{\chi}} \tag{13}$$

with $\bar{\mathbf{e}}=[\bar{e}_{\xi\xi},\bar{e}_{\eta\eta},2\bar{e}_{\xi\eta}]^T$ and $\bar{\boldsymbol{\chi}}=[\bar{\chi}_{\xi\xi},\bar{\chi}_{\eta\eta},2\bar{\chi}_{\xi\eta}]^T$.

The generalized stress components, once the kinematic model is assumed, are automatically given by assuring the invariance of the internal work. By collecting the contravariant stress components $\bar{\mathbf{S}}\equiv[\bar{S}^{\xi\xi},\bar{S}^{\eta\eta},\bar{S}^{\xi\eta}]^T$, we can write

$$\begin{aligned}\mathcal{W}&=\int_V\bar{\mathbf{S}}^T\bar{\mathbf{E}}dV=\int_\Omega\left(\bar{\boldsymbol{\mathcal{N}}}^T\bar{\mathbf{e}}+\bar{\boldsymbol{\mathcal{M}}}^T\bar{\boldsymbol{\chi}}\right)\\&=\int_\Omega\bar{\boldsymbol{\sigma}}^T\bar{\boldsymbol{\varepsilon}}d\Omega\end{aligned} \tag{14}$$

with the generalized contravariant stresses $\bar{\boldsymbol{\sigma}}\equiv[\bar{\boldsymbol{\mathcal{N}}},\bar{\boldsymbol{\mathcal{M}}}]^T$ obtained as

$$\bar{\boldsymbol{\mathcal{N}}}\equiv\int_{-t/2}^{t/2}\bar{\mathbf{S}}d\zeta\qquad\bar{\boldsymbol{\mathcal{M}}}\equiv\int_{-t/2}^{t/2}\zeta\bar{\mathbf{S}}d\zeta \tag{15}$$

and the generalized covariant strain vector $\bar{\boldsymbol{\varepsilon}}\equiv[\bar{\mathbf{e}},\bar{\chi}]^T$. Exploiting the isogeometric interpolation, $\bar{\boldsymbol{\varepsilon}}$ becomes

$$\bar{\boldsymbol{\varepsilon}}=\bar{\mathbf{A}}(\xi,\eta,\mathbf{d}_e)\mathbf{d}_e, \tag{16}$$

where $\bar{\mathbf{A}}$ depends on the displacement DOFs. This compatibility operator has the standard Green-Lagrange expression for the membrane strains, while the curvature discrete expression as well as its derivatives, which usually have very complicated formulas, are now extremely compact relations as explicitly reported in Appendix A.

2.5. The mapping between the parametric and the physical domains

For writing the constitutive equations with standard material matrices, we transform the generalized strains from the curvilinear coordinate system to a local Cartesian coordinate system whose $x-y$ plane is coincident with the mid-plane of the shell. For a general 3D continuum, this transformation is reported, for instance, in [1, 2, 29]. The simplification of this transformation accounting for the Kirchhoff-Love shell hypothesis furnishes the sought relationship:

$$\begin{aligned}\boldsymbol{\sigma}&=\mathbf{T}_\sigma\bar{\boldsymbol{\sigma}}\\\boldsymbol{\varepsilon}&=\mathbf{T}_\epsilon\bar{\boldsymbol{\varepsilon}}=\mathbf{T}_\sigma^{-T}\bar{\boldsymbol{\varepsilon}}\end{aligned}\qquad\text{with}\qquad\mathbf{T}_\sigma=\begin{bmatrix}\mathbf{T}_p&0\\0&\mathbf{T}_p\end{bmatrix} \tag{17}$$

where

$$\mathbf{T}_p=\begin{bmatrix}x_\xi^2&x_\eta^2&2x_\xi x_\eta\\y_\xi^2&y_\eta^2&2y_\xi y_\eta\\x_\xi y_\xi&x_\eta y_\eta&x_\xi y_\eta+x_\eta y_\xi\end{bmatrix} \tag{18}$$

with $x_\xi=\boldsymbol{i}_1^T\mathbf{G}_1$, $y_\xi=\boldsymbol{i}_2^T\mathbf{G}_1$, $x_\eta=\boldsymbol{i}_1^T\mathbf{G}_2$, $y_\eta=\boldsymbol{i}_1^T\mathbf{G}_2$; $\boldsymbol{i}_1$ and $\boldsymbol{i}_2$ are the unit vectors along the axis of the local Cartesian coordinates where the material properties are assigned.

Eqs.(13) and (16) in Cartesian components become respectively

$$\mathbf{E}=\mathbf{e}+\zeta\boldsymbol{\chi} \tag{19}$$

and

$$\boldsymbol{\varepsilon}=\mathbf{A}(\xi,\eta,\mathbf{d}_e)\mathbf{d}_e. \tag{20}$$

2.6. Homogenized constitutive matrix

The global behaviors of multi-layered composites, for instance deflections and buckling, can be modeled efficiently using an equivalent homogenized material based on the hypothesis of the classical lamination theory.

The homogenized material law of the shell can be expressed as

$$\boldsymbol{\sigma} = \mathbf{C}_\epsilon \boldsymbol{\varepsilon} \quad \mathbf{C}_\epsilon = \begin{bmatrix} \mathbf{C}_{ee} & \mathbf{C}_{e\chi} \\ \mathbf{C}_{e\chi}^T & \mathbf{C}_{\chi\chi} \end{bmatrix}$$

with

$$\mathbf{C}_{ee} = \sum_k t_k \mathbf{C}_k, \qquad \mathbf{C}_{e\chi} = \sum_k z_k t_k \mathbf{C}_k, \qquad \mathbf{C}_{\chi\chi} = \sum_k \left(\frac{t_k^3}{12} + t_k z_k^2 \right) \mathbf{C}_k$$

where the sum is on the number of layers, t_k is the thickness of the k-th ply and z_k is the distance between the centroid of the k-th ply and mid-plane of the laminate. In the previous equation $\mathbf{C}_k$ is the constitutive matrix of the generic lamina with respect tonthe local Cartesian frame $\{\boldsymbol{i}_1, \boldsymbol{i}_2, \boldsymbol{i}_3\}$, assumed to be orthotropic elastic and dependent on the fiber orientation.

We can note that, for generic laminations, there is a membrane-flexural coupling, which does not allow us to evaluate the membrane and the flexural strain energy separately.

High order lamination theories or layer-wise interpolations [41, 42] can be adopted for a more accurate estimate of the inter-laminar stress, which, however, is beyond the goal of this work. Some recent promising works dealt with an accurate inter-laminar stress reconstruction starting from the homogenized response, as for instance in [43], where the procedure takes advantages of the high order continuity of the solution provided by IGA.

3. Nonlinear analysis framework, numerical integration and MIP Newton's method

In this section our nonlinear analysis framework is introduced. As shown in the following, the isogeometric Kirchhoff-Love shell model may be affected by a significant locking in large deformation problems even when the initial geometry is flat, and the concept of reduced patch-wise integration is introduced for the Kirchhoff-Love model with the aim of avoiding the locking issue. The MIP Newton's method, proposed in [2, 36], is recalled and subsequently used to improve the performance of the standard Newton's method, reducing the iterative effort.

3.1. Nonlinear analysis framework

The equilibrium of slender elastic structures subject to conservative loads $f[\lambda]$ proportionally increasing with the amplifier factor λ is expressed by the virtual work equation

$$\Phi(u)' \, \delta u - \lambda f \, \delta u = 0 \quad , \quad u \in \mathcal{U} \; , \; \delta u \in \mathcal{T} \tag{21}$$

where $u \in \mathcal{U}$ is the field of configuration variables, $\Phi(u)$ denotes the strain energy, $\mathcal{T}$ is the tangent space of $\mathcal{U}$ at u and $()'$ is used to express the Fréchet derivative with respect to u. $\mathcal{U}$ is a linear manifold so that its tangent space $\mathcal{T}$ is independent of u. The discrete counterpart of Eq.(21) is

$$\mathbf{r}(\mathbf{d}, \lambda) \equiv \mathbf{s}(\mathbf{d}) - \lambda \, \boldsymbol{f} = \mathbf{0}, \quad \text{with} \quad \begin{cases} \mathbf{s}^T \delta \mathbf{d} \equiv \Phi'(u) \delta u \\ \boldsymbol{f}^T \delta \mathbf{d} \equiv f \, \delta u \end{cases} \tag{22}$$

where $\mathbf{r} : \mathbb{R}^{N+1} \to \mathbb{R}^N$ is a nonlinear vectorial function of the vector $\mathbf{z} \equiv \{\mathbf{d}, \lambda\} \in \mathbb{R}^{N+1}$, collecting the configuration $\mathbf{d} \in \mathbb{R}^N$ and the load multiplier $\lambda \in \mathbb{R}$, $\mathbf{s}[\mathbf{d}]$ is the *internal force vector* and $\boldsymbol{f}$ the *reference load vector*. Eq.(22) represents a system of N equations and $N+1$ unknowns and its solutions define the *equilibrium paths* as curves in $\mathbb{R}^{N+1}$. The Riks' approach [44] can be used to trace these curves step-by-step

from a known initial configuration $\mathbf{d}_0$ corresponding to $\lambda = 0$. At each step some Newton iterations are needed to solve (22). To this end we also define the tangent stiffness matrix as

$$\delta\mathbf{d}^T\mathbf{K}(\mathbf{d})\tilde{\mathbf{d}} = \Phi''(u)\tilde{u}\delta u \ \ , \ \ \forall\,\delta\mathbf{d}, \tilde{\mathbf{d}} \tag{23}$$

where δu and $\tilde{u}$ are generic variations of the configuration field u and $\delta\mathbf{d}$ and $\tilde{\mathbf{d}}$ the corresponding discrete vectors.

In displacement-based formulations, the strain energy can be expressed as a sum of element contributions $\Phi(u) \equiv \sum_e \Phi_e(u)$

$$\Phi_e(u) \equiv \int_{\Omega_e} \left(\frac{1}{2}\boldsymbol{\varepsilon}^T\mathbf{C}_\epsilon\boldsymbol{\varepsilon}\right) d\Omega_e \tag{24}$$

where Ω_e is the element domain. The first variation of the generalized strains in Eq.(20) can be written as

$$\delta\boldsymbol{\varepsilon} = \mathbf{B}(\mathbf{d}_e)\delta\mathbf{d}_e$$

and, then, the first variation of the strain energy is

$$\begin{aligned}\Phi_e(u)'\delta u &\equiv \int_{\Omega_e} \left(\delta\boldsymbol{\varepsilon}^T\mathbf{C}_\epsilon\boldsymbol{\varepsilon}\right) d\Omega_e \\ &= \delta\mathbf{d}_e^T \int_{\Omega_e} \left(\mathbf{B}(\mathbf{d}_e)^T\mathbf{C}_\epsilon\boldsymbol{\varepsilon}(\mathbf{d}_e)\right) d\Omega_e = \delta\mathbf{d}_e^T\mathbf{s}_e(\mathbf{d}_e)\end{aligned} \tag{25}$$

where $\mathbf{s}_e(\mathbf{d}_e)$ is the element internal force vector. The second variation of the strain measure is

$$\delta\tilde{\boldsymbol{\varepsilon}} = \mathbf{Q}(\mathbf{d}_e, \tilde{\mathbf{d}}_e)\delta\mathbf{d}_e = \mathbf{Q}(\mathbf{d}_e, \delta\mathbf{d}_e)\tilde{\mathbf{d}}_e$$

and its k-th component can be evaluated, introducing the symmetric matrix $\boldsymbol{\Psi}_k(\mathbf{d}_e)$, as

$$\delta\tilde{\varepsilon}_k = \tilde{\mathbf{d}}_e^T\boldsymbol{\Psi}_k(\mathbf{d}_e)\delta\mathbf{d}_e.$$

Letting $\boldsymbol{\sigma}(\mathbf{d}_e) = \mathbf{C}_\epsilon\boldsymbol{\varepsilon}(\mathbf{d}_e)$, the following expression holds

$$\boldsymbol{\sigma}^T\delta\tilde{\boldsymbol{\varepsilon}} \equiv \sum_k \sigma_k\delta\tilde{\varepsilon}_k = \tilde{\mathbf{d}}_e^T\boldsymbol{\mathcal{G}}(\mathbf{d}_e, \boldsymbol{\sigma}(\mathbf{d}_e))\delta\mathbf{d}_e$$

with

$$\boldsymbol{\mathcal{G}}(\mathbf{d}_e, \boldsymbol{\sigma}(\mathbf{d}_e)) = \sum_k \sigma_k(\mathbf{d}_e)\boldsymbol{\Psi}_k(\mathbf{d}_e). \tag{26}$$

The second variation of the strain energy is

$$\Phi_e''(u)\delta u\tilde{u} \equiv \int_{\Omega_e} \left(\delta\boldsymbol{\varepsilon}^T\mathbf{C}_\epsilon\tilde{\boldsymbol{\varepsilon}} + \delta\tilde{\boldsymbol{\varepsilon}}^T\boldsymbol{\sigma}(\mathbf{d}_e)\right) d\Omega_e = \delta\mathbf{d}_e^T\mathbf{K}_e(\mathbf{d}_e)\tilde{\mathbf{d}}_e \tag{27}$$

with the element tangent stiffness matrix defined as

$$\mathbf{K}_e(\mathbf{d}_e) \equiv \int_{\Omega_e} \left(\mathbf{B}(\mathbf{d}_e)^T\mathbf{C}_\epsilon\mathbf{B}(\mathbf{d}_e) + \boldsymbol{\mathcal{G}}(\mathbf{d}_e, \boldsymbol{\sigma}(\mathbf{d}_e))\right) d\Omega_e. \tag{28}$$

The discrete operators involved in the evaluation of the internal force vector and stiffness matrix are defined by means of the strain variations. The membrane part is standard while the curvature variations for the proposed model are explicitly reported in Appendix A.

3.1.1. Locking and patch-wise reduced integrations

The use of the same NURBS interpolation for all displacement components produces locking, especially for low order interpolations. In the liner elastic case, the so-called membrane locking occurs only for curved geometries, while flat plates do not exhibit any locking because the Kirchhoff model is naturally free of shear locking. However, when a Total Lagrangian formulation is used to describe the nonlinear behavior, locking may occur also for initially flat plates as a consequence of the different approximation of the terms in the nonlinear strain measure. As such, we will call this phenomenon *interpolation locking*.

Patch-wise integration rules, which take into account the inter-element high continuity of the displacement interpolation, have been proposed in recent years [5, 6] for geometrically linear problems. In our opinion, these works represent an important development in IGA.

The target space for the exact integration of a n_d-dimensional function of order q and regularity c, labeled as $\mathcal{S}_c^q$, requires a number of $n \approx ((q-c)/2)^{n_d}$ integration points per element, distributed over the patch. This number is lower than in the standard Gauss quadrature because the patch-wise integration accounts for the inter-element continuity of the function, while the Gauss quadrature assumes $c = -1$. Positions and weights are generally not equal for each element, but are evaluated, once and for all, in a pre-processing phase and depend on c, q and patch mesh. In linear elastic problems, for the full integration of the stiffness matrix terms, due to the product of the shape functions and their derivatives, we have $q = 2p$, that is twice the order of the splines, while c is the continuity order of the strains in the discrete form. The algorithms which provide these kinds of integration rules can be found in [5, 6] and are very efficient. Their computational burden is just a small fraction of the total cost of a linear analysis and negligible compared to a nonlinear analysis. We refer to [5, 6] for all details.

The patch-wise exact integration of a given space $\mathcal{S}_c^q$ also opens up new possibilities for patch-wise reduced integration schemes. In fact, q and c can be selected by the user and are not required to be those for the exact integration of the problem space. If the integration space presents spurious modes, more points than the minimum number strictly required by the space are utilized in order to remove them. In this case, the approximation space is said to be over-integrated and labeled as $\bar{\mathcal{S}}_c^q$. With respect to the element-wise reduced integration, an appropriate selection of the patch-wise reduced integration rule makes it possible to alleviate or eliminate locking in the linear elastic range avoiding spurious modes and further reduce the number of integration points [5, 6].

Different patch-wise integration rules in large deformation problems have been investigated in [2, 29] for a solid-shell formulation. Excellent results in terms of locking reduction and efficiency has been obtained for C^2 NURBS.

So far, the use of patch-wise reduced integration rules for the Kirchhoff-Love shell model in large deformations has not been assessed to our knowledge. For this reason, in the following we carry out a numerical investigation on different patch-wise integration rules for this shell model with the aim of looking for an optimal NURBS order-integration space solution in terms of accuracy, efficiency and robustness.

Given that in patch-wise rules the number of integration points n can be different element-by-element, the internal force vector can be evaluated as

$$\mathbf{s}_e(\mathbf{d}_e) = \sum_g^n \left(\mathbf{B}_g(\mathbf{d}_e)^T \mathbf{C}_g \boldsymbol{\varepsilon}_g(\mathbf{d}_e) \right) w_g \tag{29}$$

while the tangent stiffness matrix is

$$\mathbf{K}_e(\boldsymbol{\sigma}_g(\mathbf{d}_e), \mathbf{d}_e) = \sum_g^n \left(\mathbf{B}_g(\mathbf{d}_e)^T \mathbf{C}_g \mathbf{B}_g(\mathbf{d}_e) + \boldsymbol{\mathcal{G}}_g(\mathbf{d}_e, \boldsymbol{\sigma}_g(\mathbf{d}_e)) \right) w_g \tag{30}$$

where subscript g denotes quantities evaluated at the integration point $\boldsymbol{\xi}_g$, w_g is the product of the corresponding weight and the determinant of the Jacobian matrix $\mathbf{J}$ evaluated at the integration point, $\mathbf{C}_g$ is $\mathbf{C}_\epsilon$ at the integration point.

Note that $\mathbf{K}_e(\mathbf{d}_e)$ is written as $\mathbf{K}_e(\boldsymbol{\sigma}_g(\mathbf{d}_e), \mathbf{d}_e)$ as a reminder of the way it is computed.

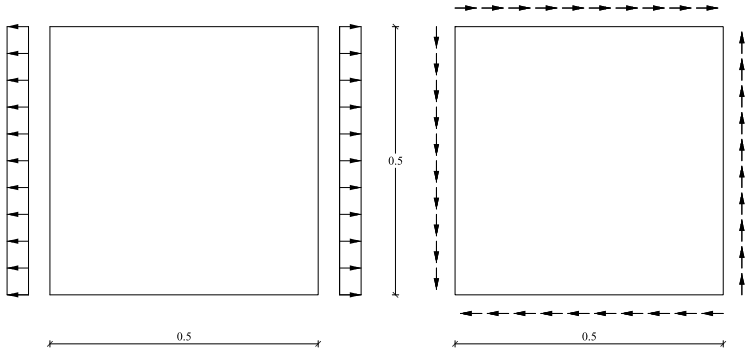

Figure 2: Simple plane stress problems: geometries and loads.

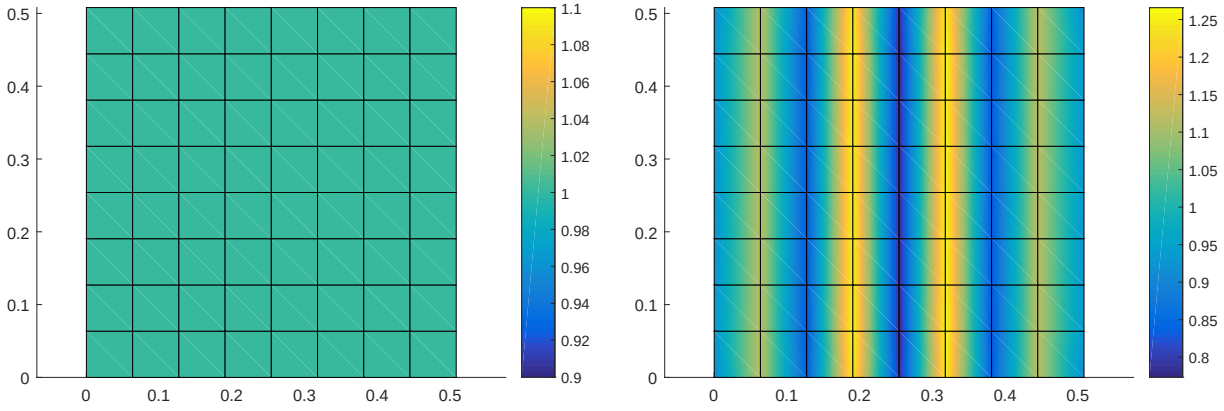

(a) $\mathcal{S}_0^4$ and $\bar{\mathcal{S}}_0^2$ solution, $\frac{u_{\max}}{u_{\max}^{\text{exact}}} = 1$

(b) $\mathcal{S}_1^4$ solution, $\frac{u_{\max}}{u_{\max}^{\text{exact}}} = 1.0125$

Figure 3: Simple plane stress tensile problem: N_{xx} solution.

3.1.2. Remarks on the continuity of reduced integration space

The use of a reduced integration space in IGA was firstly assessed in [6], where the authors state the possibility of using an integration space with continuity c equal or greater than the continuity of the strains, but advise against the case of c greater than the continuity of the strains because of its lower accuracy. We want to make a remark on this aspect, which will be useful for choosing the reduced integration spaces of the present model.

According to our numerical experience, the integration space continuity cannot be greater than the strain one to assure the exact evaluation of constant stress states. A simple example is exploited to support this statement, consisting of the two simple linear elastic plane stress problems depicted in Fig.2, whose exact solution corresponds to constant stresses. For the problem under consideration, when C^1 quadratic B-splines are employed, the strains are C^0 continuous and, then, the full integration space for the stiffness matrix is $\mathcal{S}_0^4$. As shown in Figs. 3 and 4, the full integration scheme $\mathcal{S}_0^4$ and the reduced one $\bar{\mathcal{S}}_0^2$ furnish the exact stress state. Conversely, the stress solution is no longer constant when the integration space $\mathcal{S}_1^4$ is used.

For the Kirchhoff-Love shell model, the strain energy has a continuity equal to the spline order minus 2 (second derivative of the displacements in the strain measure). This means that, when using C^1 and C^2 splines, the full integration spaces for the linear elastic case are $\mathcal{S}_{-1}^4$ and $\mathcal{S}_0^6$, respectively, where $r = -1$ means discontinuity. Keeping in mind the results of the previous example, in selection of the integration spaces it is necessary to maintain $r = -1$ and $r = 0$ in the integration space of C^1 and C^2 splines, respectively. For discontinuous spaces ($r = -1$), the integration is no longer patch-wise but is carried out at the element level and then coincides with the standard Gauss quadrature. This means that 3×3 Gauss points are needed to fully integrate the C^1 case and the only possibility of reduced integration without spurious modes is using

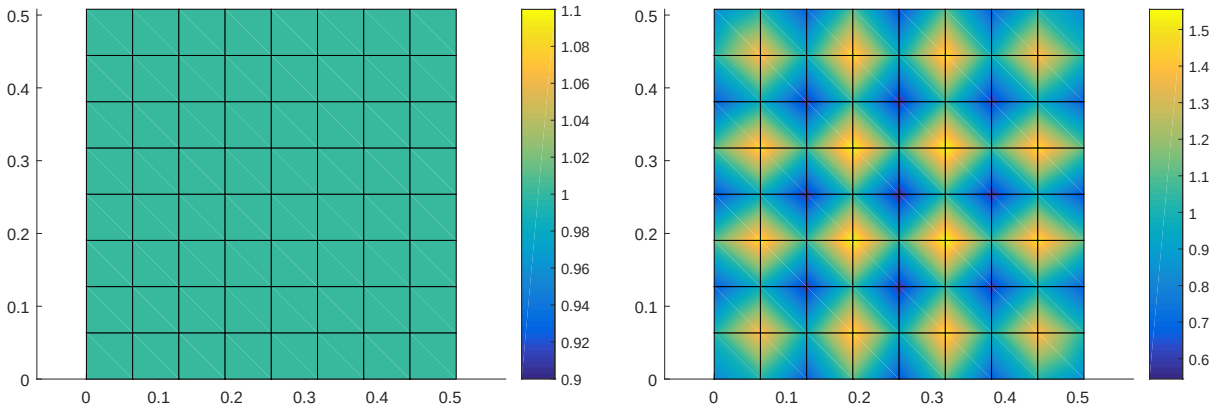

(a) $\mathcal{S}_0^4$ and $\bar{\mathcal{S}}_0^2$ solution, $\frac{u_{\max}}{u_{\max}^{\text{exact}}} = 1$

(b) $\mathcal{S}_1^4$ solution, $\frac{u_{\max}}{u_{\max}^{\text{exact}}} = 1.0457$

Figure 4: Simple plane stress shear problem: N_{xy} solution.

2×2 Gauss points. The $\bar{\mathcal{S}}_0^2$ space, which in solid-shell models is the most suitable choice for quadratic splines [2, 29], is added in some numerical examples to show the non-convergent behavior for Kirchhoff-Love shells due to the excessive continuity. As shown in the following, this is a relevant limitation of second order splines for this structural model. Concerning C^2 splines, the reduced integration spaces $\mathcal{S}_0^3$ and $\mathcal{S}_0^4$ will be assessed.

3.2. The iterative scheme with mixed integration points

The isogeometric shell model proposed in section 2 with the patch-wise reduced integration is accurate and efficient and represents a reliable choice from the point of view of the discrete approximation and the efficiency of the integration. However, the efficiency and the robustness of a nonlinear analysis do not only depend on the number of unknowns and integration points, but also on the iterative effort, that is on the capability of the Newton's method to converge using a low number of iterations and to withstand large step sizes (increments). In [34, 35], it is shown that the Newton's method exhibits a slow convergence and requires a small step size for slender elastic structures undergoing large displacements when any purely displacement-based formulation is adopted. This could be considered as a sort of "locking" of the Newton's method, since its performance gets worse when the slenderness of the structure increases. This fact is unrelated to the accuracy of the interpolation and always occurs in displacement formulations because the stresses $\boldsymbol{\sigma}_g(\mathbf{d}_e)$, used to evaluate the tangent stiffness matrix $\mathbf{K}_e(\boldsymbol{\sigma}_g(\mathbf{d}_e), \mathbf{d}_e)$, are forced to satisfy the constitutive equations at each iteration. Conversely, mixed (stress-displacement) formulations are not affected by this phenomenon, because the stresses are directly extrapolated and corrected in the iterative process, allowing a faster convergence of the Newton's method and very large steps, independently of the slenderness of the structure. We refer readers to [34, 35] for further details on this.

In [36] a strategy called Mixed Integration Point (MIP) has been proposed in order to overcome these limitations in standard displacement-based finite element problems and then extended and tested in displacement-based isogeometric formulations [2, 37, 38]. The fundamental idea of the MIP Newton scheme is to relax the constitutive equations at the level of each integration point during the iterations. Details on the method formulation are reported in [2, 36].

The modified version of the Newton's method evaluates and decomposes the iteration matrix at the first extrapolation (predictor) of each step and represents an attractive choice if the method converges in a reasonable number of iterations. The MIP Newton, even in the modified version, is more robust and requires a lower number of iterations compared to the traditional full Newton's method [36]. In IGA, the modified version of the method seems even more attractive then in low order finite element formulations for two reasons. The first one is that the number of stiffness matrix evaluations, which involve integration and assembly, becomes much lower and, in IGA, this represents a significant part of the cost of the analysis.

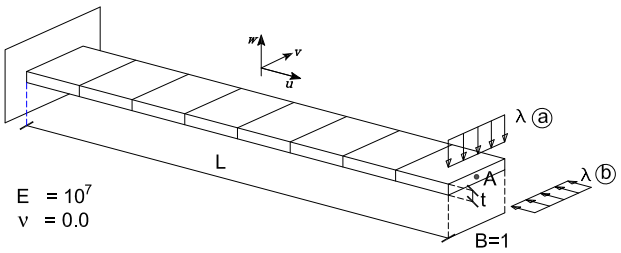

Figure 5: Cantilever beam under two load cases: geometry and loads.

The second reason is that the ratio between the cost of an iteration performed with a new matrix and its cost using an already decomposed one is directly proportional to the band. This means that the modified Newton's method becomes more and more competitive as the order of the NURBS, and then the band of the matrix, increases.

4. Numerical results

In this section, the accuracy of the proposed isogeometric Kirchhoff-Love shell model with C^1 and C^2 NURBS interpolation and different patch-wise integration schemes is tested in large deformation problems, along with the the performance of the MIP strategy. Shell structures in both isotropic and composite multi-layered materials are considered. Comparisons with other IGA shell models is reported. The simplified strain measure is tested and compared with the exact Kirchhoff-Love one and a solid-shell solution (SS).

4.1. Interpolation locking tests

Some simple large deformation problems are herein considered to show the occurrence of interpolation locking in the isogeometric Kirchhoff-Love model, which may be present also in flat plates and is related to the slenderness of the shell.

A series of patch-wise exact and reduced integration schemes for C^1 and C^2 NURBS bases are employed and compared. In order to show the performance of the different strategies in dealing with locking, the simple cantilever beam depicted in Fig. 5 is analyzed for different values of the slenderness parameters $k = L/t$ and under two different load conditions.

4.1.1. Cantilever beam under shear force

For the shear load case, Fig. 6 shows the equilibrium paths, up to the maximum value of the load $\lambda_{max} = 4 \cdot 10^7/k^3$, obtained with the C^1 interpolation for two different values of $k = 100$ and $k = 1000$ and different meshes.

The full 3×3 Gauss Point (GP) integration scheme presents an evident locking and provides bad results also for the smallest value of k, unless 16 elements are used. Locking gets more evident for $k = 1000$ and makes the fully integrated prediction far from the exact solution even for the finest mesh employed. This a clear example that, when moving from linear analysis to large deformation problems, interpolation locking occurs for the discrete Kirchhoff-Love shell model even if the initial geometry is flat. The 2×2 GP reduced integration shows a better performance, but it is still not satisfactory for the slenderness $k = 1000$, when it requires a fine mesh to get a good prediction. The results are compared also with a solid-shell model integrated by $\bar{\mathcal{S}}_0^2$, which provides, at convergence, the same prediction. Its results are quite worse for the coarsest mesh because of the over-integration penalization, but it behaves better for finer meshes. We have however to remember that the solid-shell model has twice the DOFs of the Kirchhoff-Love one for a given mesh.

For the C^2 interpolation, the equilibrium paths of the cantilever beam under shear load discretized with 4 and 8 elements are reported in Fig. 7. Also in this case, the full integration S_0^6 is clearly affected by locking. On the contrary, the integration scheme S_0^3 provides excellent results. It shows a locking-free solution even

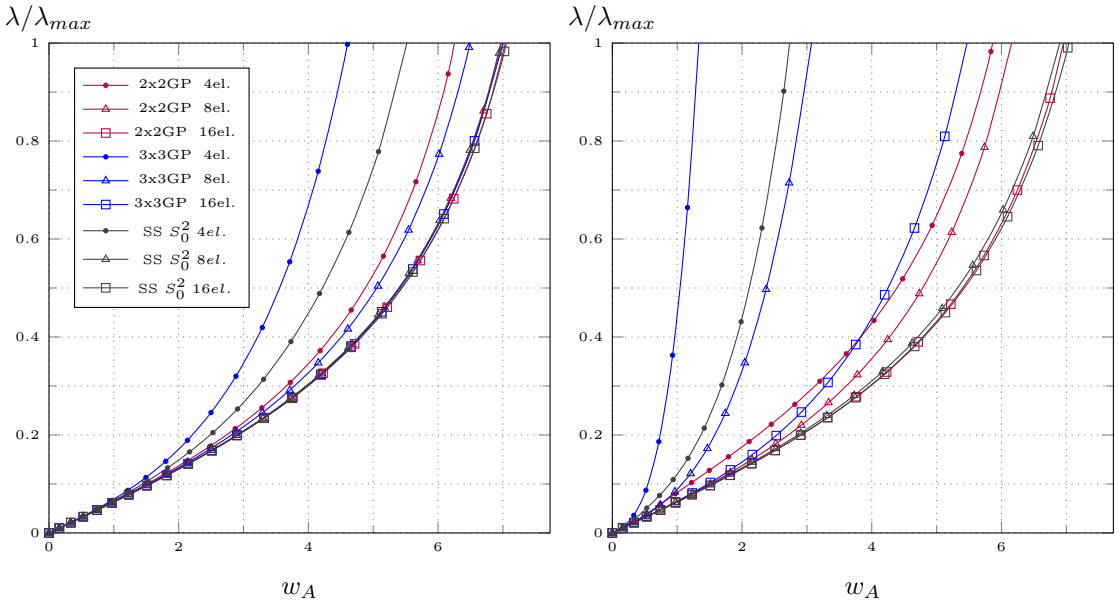

Figure 6: Cantilever beam under shear force: equilibrium path for C^1 and $L/t = 100$ (left) and $L/t = 1000$ (right).

for the coarsest mesh. It is worth noting that S_0^3 requires the lowest number of integration points (about 2.25 per element) and is very efficient compared with Gauss rules. For comparison, the results using a solid-shell element integrated with S_1^4 [2, 29] are reported as well. Also in this case the final prediction of the two structural models is the same, with the solid-shell element slightly more sensitive to locking for coarse meshes. Finally we note that the simplified KL strain measure provides the same equilibrium path as the one obtained with the solid-shell element proposed in [2, 29] and based on a full 3D Green-Lagrange strain measure, as it can be observed in Figs. 6 and 7.

In Tab. 1 the results previously described are summarized reporting the value of the end beam displacement w_A corresponding to a unitary load normalized with respect to the reference values w_A^{ref} obtained with C^2 interpolation, 32 elements and a S_0^3 integration. The table makes the comparison of the different strategies easy and highlights the great accuracy and insensitivity to locking of the C^2 interpolation when integrated with S_0^3, as well as the significant qualitative leap when passing from C^1 to C^2. We can note that for the C^1 case the $\bar{S}_0^2$ integration does not converge to the correct deflection, due to the observation drawn in 3.1.2.

When comparing the computational effort of C^1 and C^2 formulations for a given mesh, we have to note that the C^2 one has a very slightly higher number of DOFs, which gets negligible for large meshes, and leads to a band of the stiffness matrix almost twice as large. However, the reduction of integration points, made possible by the integration space continuity, makes the C^2 cost quite near to the C^1 case. Considerations similar to C^2-S_0^3 holds for C^2-S_0^4, which however exhibits a slight locking.

The use of the C^2 interpolation with the S_0^3 integration scheme seems then to be the optimal choice, since it is able to provide excellent predictions with very coarse meshes, independently on the slenderness.

4.1.2. Cantilever beam under compression

The second test regards the same cantilever beam under compression, i.e., a standard Euler cantilever beam. A very small shear imperfection load is added to avoid the jump of the bifurcation. The equilibrium path for different discretizations, integration schemes and slenderness ratios are reported in Fig. 8 for the C^1 interpolation and in Fig. 9 for the C^2 one. The load factor is normalized with respect to the analytical buckling load λ_b. Similar comments to the previous test hold. In particular, the reduced integration schemes 2×2 for C^1 behaves much better than the full integration, but it is still not satisfactory for the more

		4 elm.				8 elm.				16 elm.			
	L/t	$\bar{S}_0^2$	S_0^3	S_0^4	2x2GP	$\bar{S}_0^2$	S_0^3	S_0^4	2x2GP	$\bar{S}_0^2$	S_0^3	S_0^4	2x2GP
C^1	10^2	0.876	0.970	0.651	0.887	1.016	0.971	0.923	0.989	1.019	1.000	1.000	0.999
	10^3	0.874	0.972	0.190	0.831	1.015	0.968	0.435	0.873	1.018	0.966	0.776	0.987
	L/t	S_0^3	S_0^4	S_0^5	S_0^6	S_0^3	S_0^4	S_0^5	S_0^6	S_0^3	S_0^4	S_0^5	S_0^6
C^2	10^2	0.994	0.994	0.973	0.963	1.000	0.999	0.999	0.999	1.000	1.000	1.000	1.000
	10^3	0.994	0.944	0.838	0.833	0.999	0.991	0.956	0.952	1.000	0.999	0.998	0.998

Table 1: Cantilever-beam: normalized end displacement at $\lambda/\lambda_{max} = 1$ for different interpolations and slenderness.

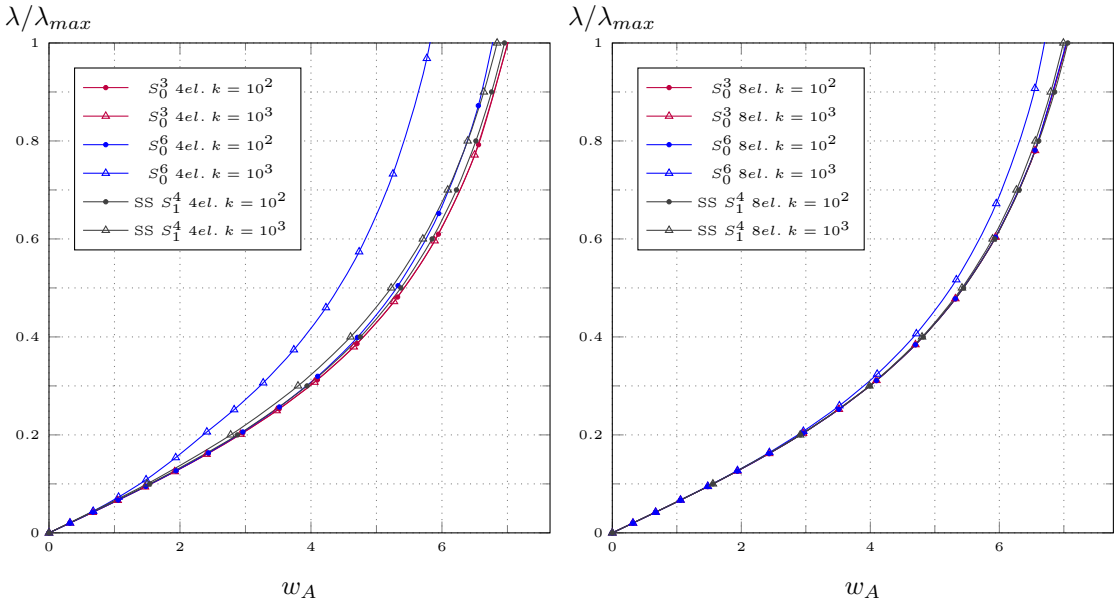

Figure 7: Cantilever beam under shear force: equilibrium path for C^2 with 4 and 8 elements.

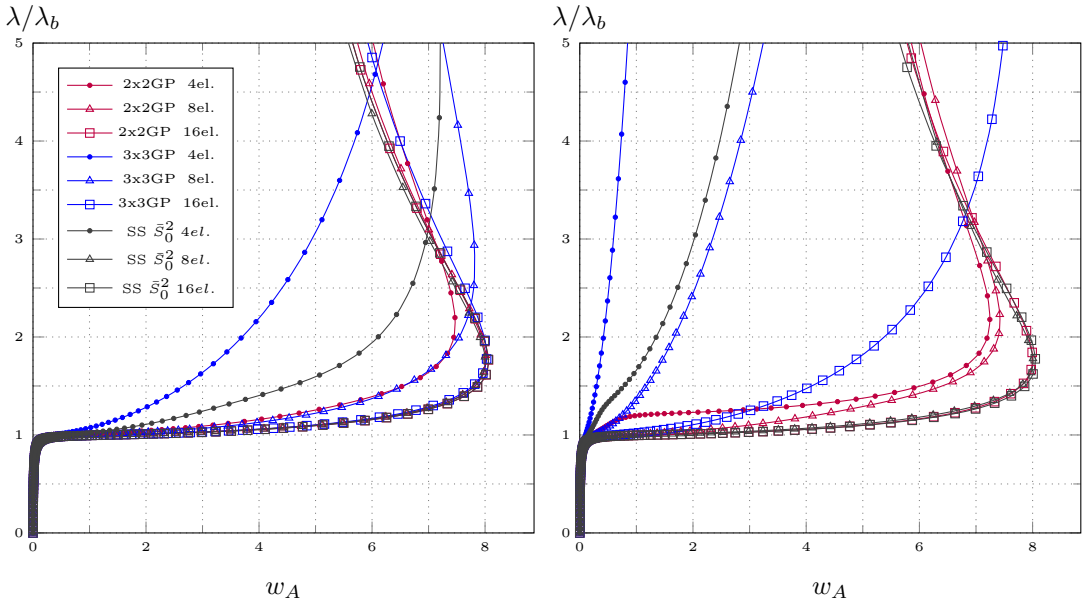

Figure 8: Cantilever beam under compression: equilibrium path for C^1 and $L/t = 10^2$ (left) and $L/t = 10^3$ (right).

slender case because of some residual locking. Conversely, S_0^3 with C^2 provides good predictions, practically insensitive to k even for a very coarse mesh. Finally, the C^2 interpolation outperforms the C^1 one again in terms of accuracy, using the same mesh, and then employing a similar number of DOFs and a lower number of integration points. The comparison with the solid-shell results show again that the simplified strain measure does not lead to a loss in accuracy also for very large displacements. Concerning the discrete approximation, the solid-shell C^1-$\bar{S}_0^2$ solution is penalized for very coarse meshes by the over integration while C^2-S_1^4 solid-shells provide results comparable to the C^2 Kirchhoff-Love elements integrated with S_0^3, but use a twice as big number of DOFs per element.

We can conclude that the C^2 interpolation seems preferable to the C^1 due to the possibility of also using coarse meshes when integrated with the S_0^3, which is insensitive to locking also for very slender structures and needs a low number of integration points. Other numerical tests will be presented in the next section to further validate this proposal.

4.2. A simple test for the MIP Newton

To highlight the robustness and the efficiency of the proposed MIP strategy, the equilibrium path of the example in Fig. 7 under a shear load has been reconstructed using a load-controlled scheme. The maximum load value has been subdivided into $Nsteps$ equal load increments. The total number of iterations required to evaluate the equilibrium path with different strategies, but under the same convergence criteria, are reported in Tab. 2.

The performance of the standard Newton method clearly depends on the slenderness of the beam. In particular, its robustness in terms of increment size worsens when the ratio $k = L/t$ increases, and the method is not able to converge for $k = 10^4$ and requires 5 increments to converge for $k = 10^3$. Conversely, the MIP Newton is able to evaluate the equilibrium point corresponding to $\lambda = \lambda_{max}$ with just a single load increment and only 5 iterations. When the number of load steps $Nsteps$ increases, the number of iterations per step gets smaller, but the total number of iterations increases. However, even for the smallest step size the MIP Newton is more than twice as efficient as the standard Newton. Finally, even the modified MIP Newton withstands the largest step size with a single matrix decomposition. Moreover, it requires a number of iterations tending towards that of the full MIP Newton when the step size decreases. It is clear that the modified method represents a very attractive choice, considering that its computational cost is dominated

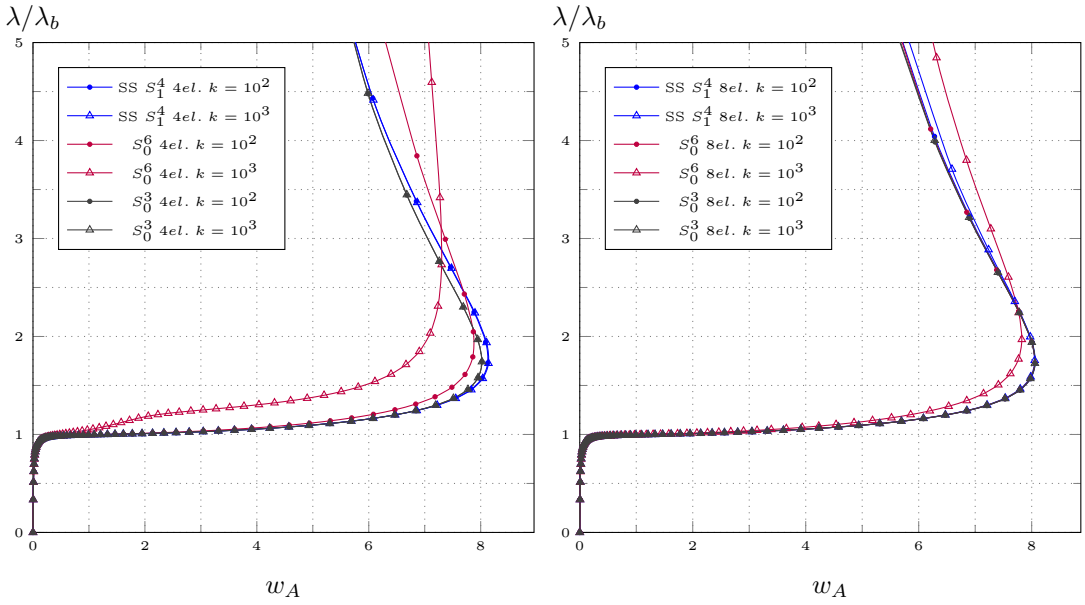

Figure 9: Cantilever beam under compression: equilibrium path for C^2 with 4 and 8 elements.

	Newton			MIP Newton			MIP M. Newton		
	k			k			k		
N_{steps}	10^2	10^3	10^4	10^2	10^3	10^4	10^2	10^3	10^4
1	14	fails	fails	5	5	5	15	15	15
5	40	49	fails	16	16	17	21	21	21
10	60	83	fails	30	30	30	32	33	35
20	98	121	fails	51	51	51	51	51	54

Table 2: Cantilever beam under shear force ($C^2 - S_0^3$, $L/t = 10^2, 10^3$): total number of iterations for the evaluation of the equilibrium path vs the number of load subdivisions.

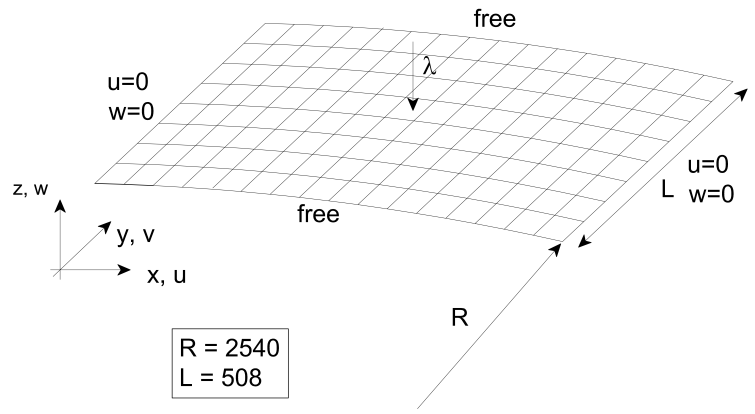

Figure 10: Shallow roof: geometry and boundary conditions.

E_{11}	$E_{22} = E_{33}$	$\nu_{12} = \nu_{13} = \nu_{23}$	$G_{12} = G_{13}$	G_{23}
3300	1100	0.25	660	440

Table 3: Composite shallow roof: material properties.

by the number of matrix decompositions and so of increments, not of iterations. Finally, it is interesting to note that the convergence of both the full and the modified MIP Newton are unrelated to the slenderness k and, in our opinion, this represents the main advantage of the MIP strategy.

4.3. Hinged cylindrical shallow roof

The benchmark depicted in Fig. 10 is analyzed in both the isotropic case with $E = 3102.75$, $\nu = 0.3$ and in the multi-layered cases [0/90/0] and [90/0/90] with the material properties reported in Tab. 3. Two different thickness of $t = 12.7$ and $t = 6.35$ are considered because they are characterized by different behaviors.

4.3.1. Thickness $t = 12.7$

Figure 11 reports, for the isotropic case, the equilibrium paths obtained using different meshes of C^1-2×2GP and C^2-S_0^3 elements and compares the results with those obtained with C^1-$\bar{S}_0^2$ and C^2-S_1^4 solid-shell elements respectively. It is possible to observe that a grid of 4×4 C^2-S_0^3 elements is enough to obtain the exact path.

In Fig. 12 the equilibrium paths for all considered materials are reported to show that the exact and the SKL models give the same results also for large displacements.

The convergence to the reference solution and the possibility to employ very coarse meshes is highlighted in Fig. 13 for C^1 NURBS and Fig. 14 for C^2 NURBS. In these figures, the equilibrium paths for different material layups are evaluated with the SKL model and compared with the solid-shell converged solution. It is possible to observe that the influence of the shear flexibility, accounted for in the solid-shell solution, seems to be negligible in the equilibrium path. In Fig.15 the deformed shapes for the different material cases at limit points are reported.

4.3.2. Thickness $t = 6.35$

This thickness is analyzed only for laminated materials and presents a more complex equilibrium path as reported in Figs. 16 and 17. However, a mesh of 8×8 SKL C^2-S_0^3 elements is able to provide results coincident with the reference solid-shell solution. The deformed shapes for the different material cases at limit points are shown in Fig. 18.

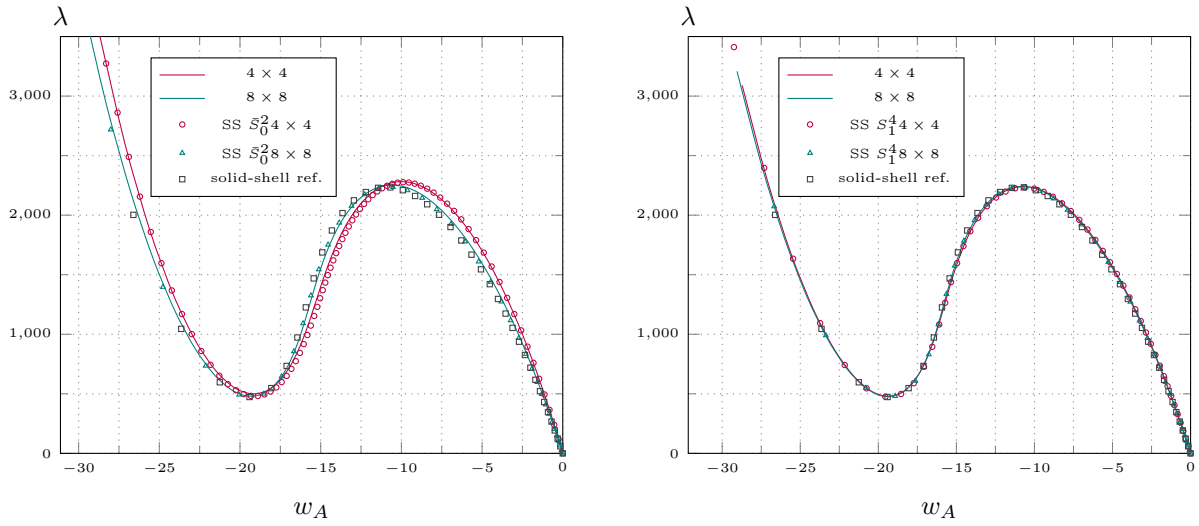

Figure 11: Isotropic shallow roof: equilibrium paths with element C^1-2x2GP (left) and C^2-S_0^3 (right) for $t = 12.7$

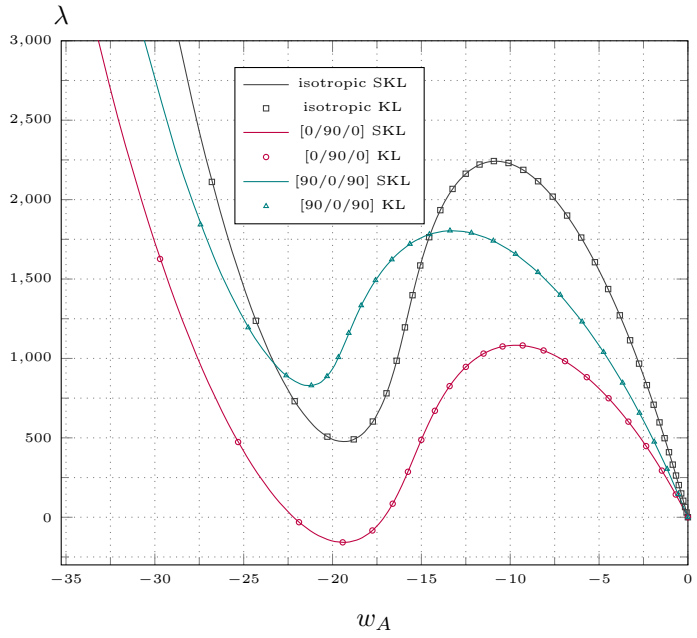

Figure 12: Laminated shallow roof: equilibrium paths for 8×8 C^2-S_0^3 elements for $t = 12.7$.

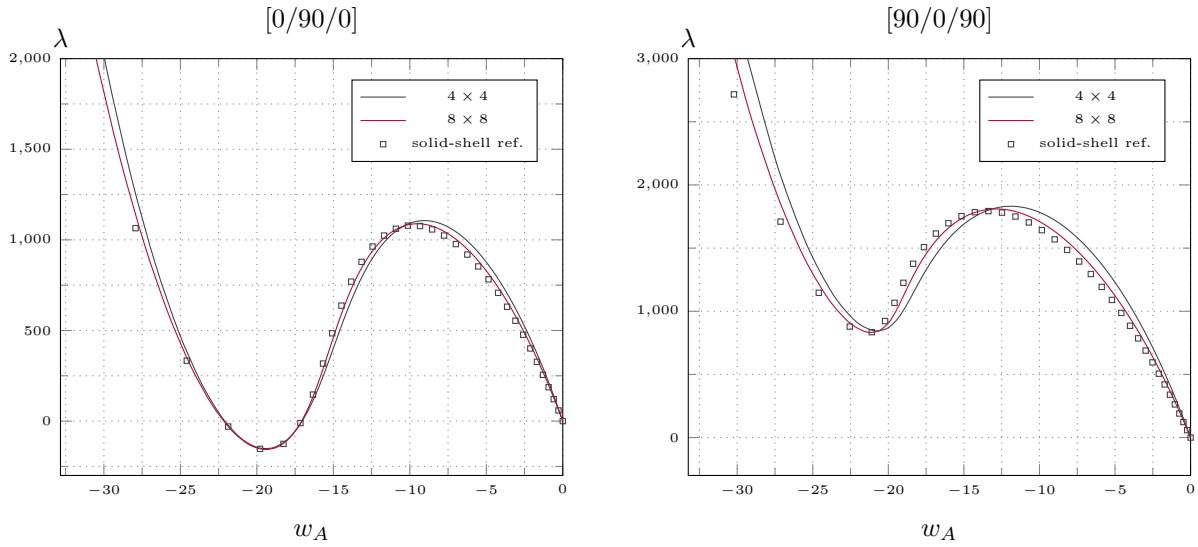

Figure 13: Laminated shallow roof: equilibrium paths with element C^1-2x2GP for different meshes and layups for $t = 12.7$

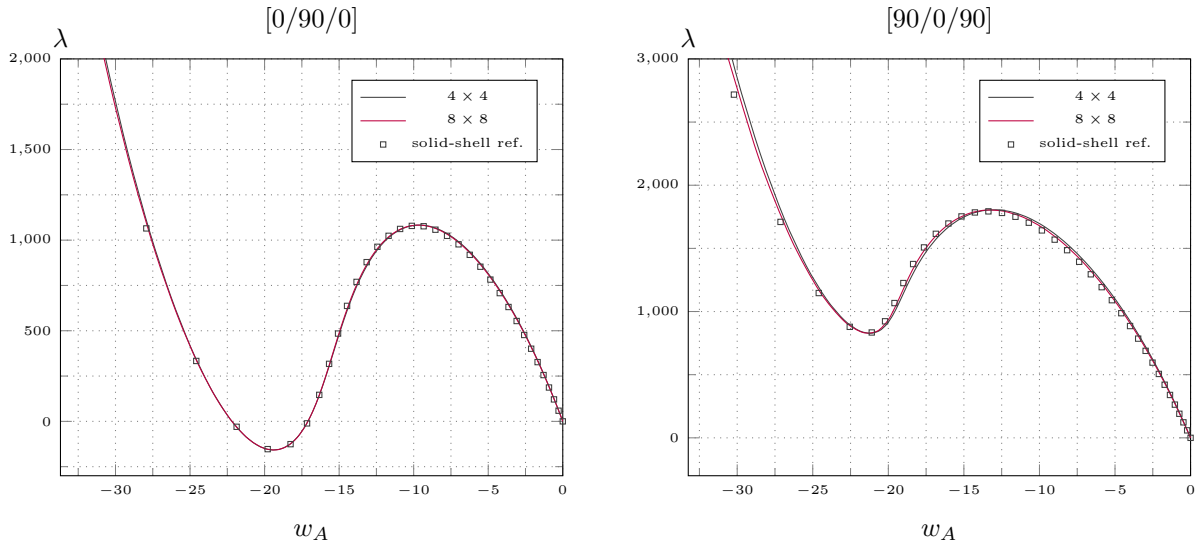

Figure 14: Laminated shallow roof: equilibrium paths with element C^2-S_0^3 for different meshes and layups for $t = 12.7$

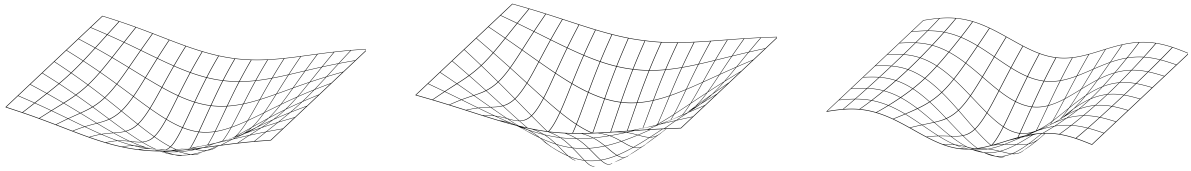

(a) isotropic (b) [90/0/90] (c) [0/90/0]

Figure 15: Shallow roof: deformed shapes (scale factor = 15) at limit point for different layups and $t = 12.7$.

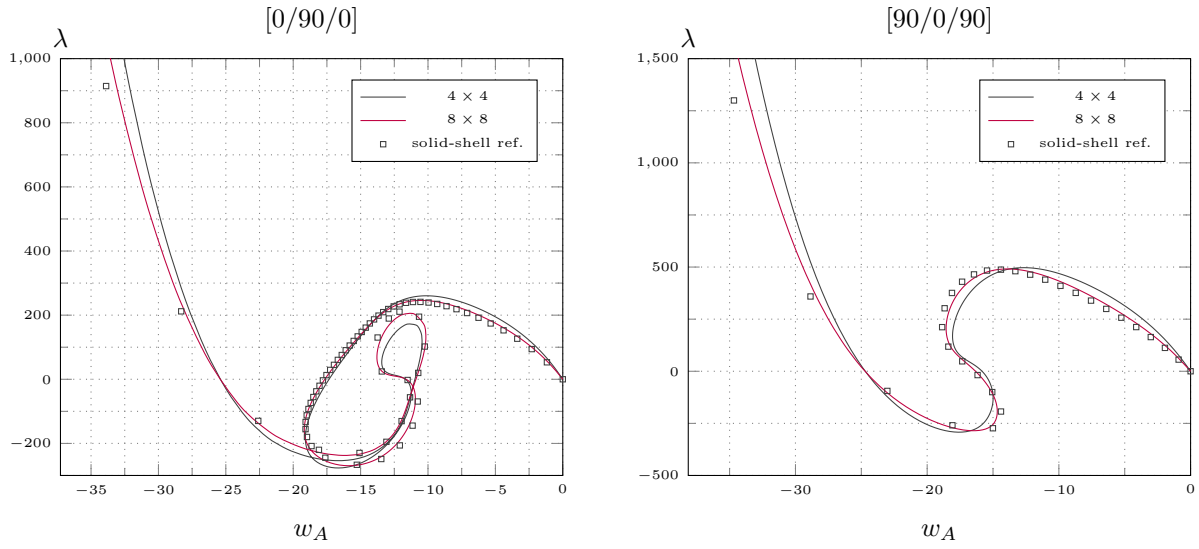

Figure 16: Laminated shallow roof: equilibrium paths with element C^1-2x2GP for different meshes and layups for $t = 6.35$

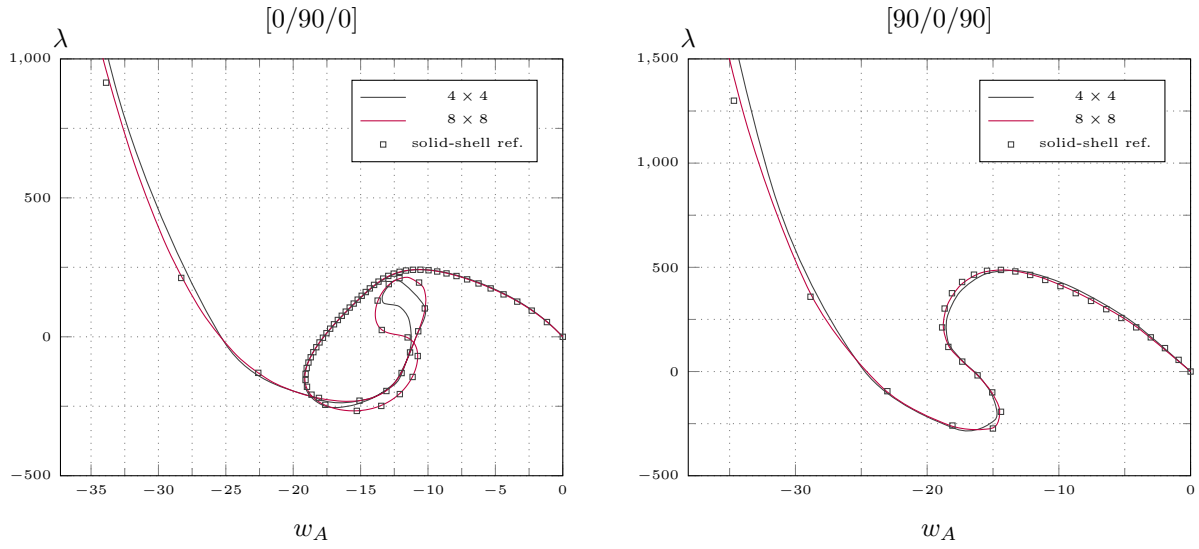

Figure 17: Laminated shallow roof: equilibrium paths with element C^2-S_0^3 for different meshes and layups for $t = 6.35$

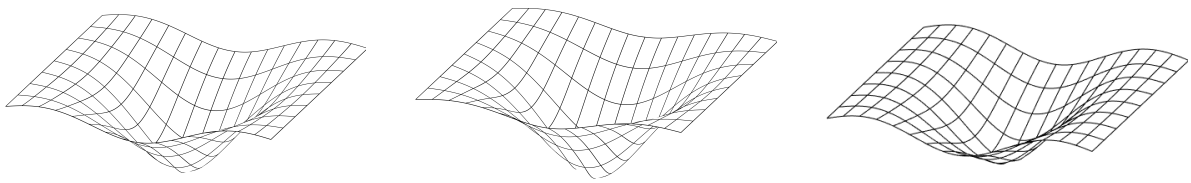

(a) isotropic (b) [90/0/90] (c) [0/90/0]

Figure 18: Shallow roof: deformed shapes (scale factor = 15) at limit point for different layups and $t = 6.35$.

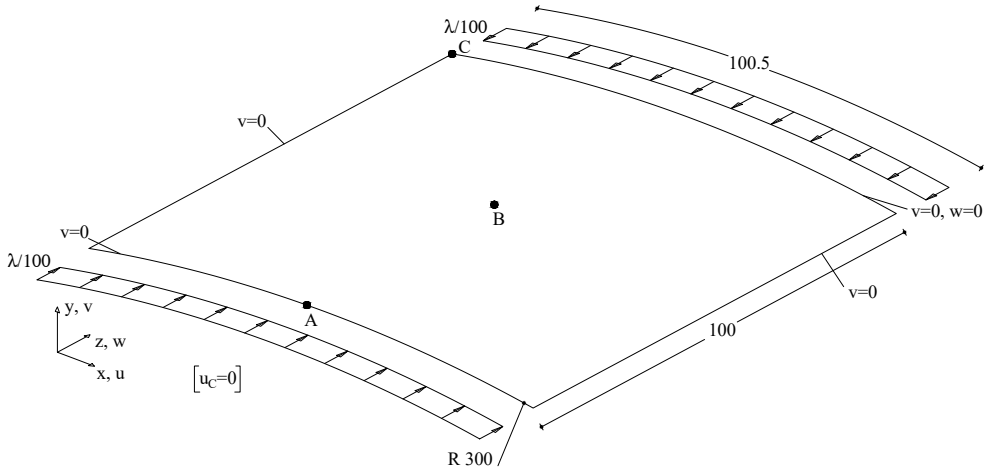

Figure 19: Composite curved panel: geometry and boundary conditions.

E_{11}	$E_{22} = E_{33}$	$\nu_{12} = \nu_{13}$	ν_{23}	$G_{12} = G_{13}$	G_{23}
30.6	8.7	0.29	0.5	3.24	2.9

Table 4: Composite curved panel: material properties.

4.4. Composite curved panel under compression

This test consists of the stability analysis of a composite curved panel subjected to an axial compression, as described in Fig. 19. The laminated is composed of six layers with material properties reported in Tab. 4. Two lamination are considered: $[0]_6$ and $[45/-45/0]_s$. The same example has been already analyzed in [29] using an isogeometric version of the Koiter method and a solid-shell model in [45], which dealt with the layup optimization with respect to the post-buckling response. Firstly, a linearized buckling analysis of the perfect structure is carried out. The lowest eight eigenvalues are reported in Tabs. 5 and 6 for the two laminations, while some modal shapes are depicted in Fig. 20. The eigenvalues are shown for C^1 and C^2 NURBS using various discretizations and integration schemes. They are normalized with respect to a reference solution obtained with 64×64 C^2-S_0^3 elements. The high continuity together with the exact representation of the geometry leads to very good results with all integration strategies. The comparison includes also the influence of the strain measure. No relevant difference between the proposed simplified Kirchhoff-Love model and the exact one can be observed.

The study of the post-buckling response of the panel is carried out considering the presence of a geometrical imperfection $\mathbf{d}^*$ that is a combination of the first and the second buckling modes. In particular, it is the difference between them scaled in order to obtain $\|\mathbf{d}^*\|_\infty = 0.1t$. The equilibrium curves are illustrated in Figs. 21 and 22 for $[0]_6$ and $[45/-45/0]_s$ respectively. They exhibit a limit point and a snap-through behavior. We can note the great accuracy of the proposed isogeometric analysis even for an extremely coarse mesh, in particular for the C^2-S_0^3 element. The equilibrium paths provided by the proposed model are assessed by means of a comparison with a geometrically exact C^2 solid-shell model using a mesh of 32×32 and a S_1^4 integration scheme. We can conclude that the simplified version of the Kirchhoff-Love model is as accurate as other objective models in predicting the behavior of slender panels, even for large displacements. Finally, Tab. 7 reports the total number of steps and iterations needed to trace the above mentioned equilibrium curves up to a maximum displacement equal to 5. The superior efficiency and robustness of the MIP Newton is evident also for this test, especially for the modified version which is about 4 and 5 times more efficient than the standard full Newton for $[0]_6$ and $[45/-45/0]_s$ respectively, requiring a significant lower number of stiffness matrix evaluations and factorizations.

Model	4 elm.		8 elm.		16 elm.	
	C^1-2 × 2GP	C^2-S_0^3	C^1-2 × 2GP	C^2-S_0^3	C^1-2 × 2GP	C^2-S_0^3
SKL	1.032	0.957	1.007	0.996	0.997	1.000
	1.097	0.975	1.024	0.997	1.003	1.000
	1.176	0.978	1.032	0.995	1.007	0.999
	1.245	0.986	1.031	0.997	1.007	1.000
	1.263	0.987	1.079	1.004	1.017	1.000
	1.300	0.994	1.083	1.002	1.020	1.000
	1.378	1.246	1.067	0.995	1.014	1.000
	1.331	1.149	1.084	1.000	1.019	1.000
KL	1.031	0.957	1.007	0.995	0.997	0.999
	1.097	0.975	1.024	0.997	1.003	1.000
	1.176	0.977	1.032	0.995	1.007	0.999
	1.245	0.985	1.031	0.997	1.006	0.999
	1.263	0.986	1.079	1.004	1.017	1.000
	1.300	0.994	1.083	1.002	1.020	1.000
	1.378	1.246	1.067	0.994	1.014	1.000
	1.331	1.149	1.084	1.000	1.019	1.000

Table 5: Composite curved panel: first 8 normalized buckling loads for $[0]_6$

Model	4 elm.		8 elm.		16 elm.	
	C^1-2 × 2GP	C^2-S_0^3	C^1-2 × 2GP	C^2-S_0^3	C^1-2 × 2GP	C^2-S_0^3
SKL	1.052	0.985	1.027	1.002	1.005	1.000
	1.048	0.984	1.024	1.002	1.003	1.000
	1.106	0.967	1.023	1.001	1.001	1.000
	1.151	1.027	1.076	1.004	1.025	1.000
	1.148	1.052	1.058	1.001	1.008	1.000
	1.165	1.176	1.074	1.004	1.016	1.000
	1.238	1.606	1.093	1.005	1.042	1.001
	1.237	1.596	1.092	0.999	1.010	1.000
KL	1.052	0.985	1.027	1.002	1.005	1.000
	1.048	0.984	1.024	1.002	1.003	1.000
	1.106	0.967	1.023	1.001	1.001	1.000
	1.151	1.027	1.076	1.004	1.025	1.000
	1.148	1.052	1.058	1.001	1.008	1.000
	1.165	1.176	1.074	1.004	1.016	1.000
	1.238	1.606	1.093	1.005	1.042	1.001
	1.237	1.596	1.092	0.999	1.010	1.000

Table 6: Composite curved panel: first 8 normalized buckling loads for $[45/-45/0]_s$

	Newton		MIP Newton		MIP M. Newton	
layup	steps	iters	steps	iters	steps	iters
$[0]_6$	58	180	46	134	46	134
$[45/-45/0]_s$	65	226	46	137	47	141

Table 7: Laminated curved panel: total number of steps and iterations for the evaluation of the equilibrium path using 8×8 C^2-S_0^3 elements.

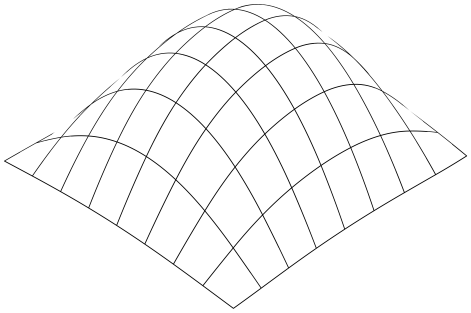

(a) mode 1 $[0]_6$

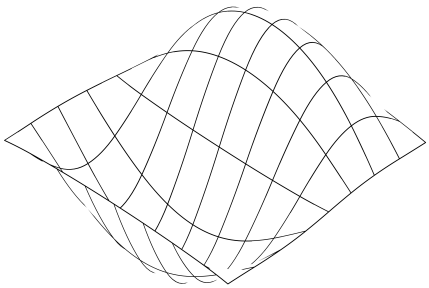

(c) mode 2 $[0]_6$

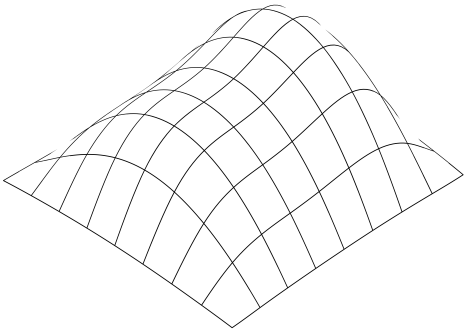

(b) mode 1 $[45/-45/0]_s$

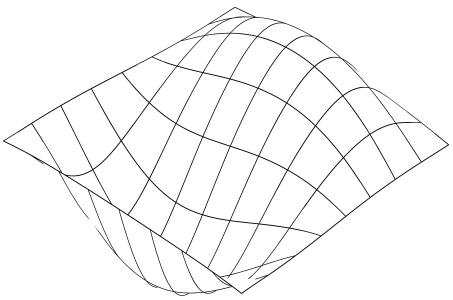

(d) mode 2 $[45/-45/0]_s$

Figure 20: Composite curved panel: first and second buckling mode corresponding to two different layups

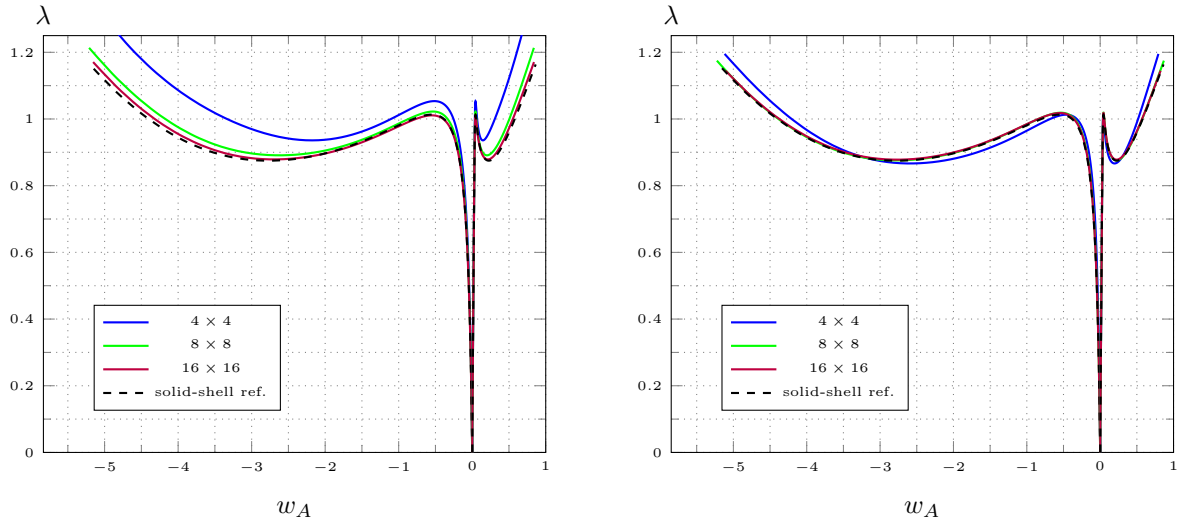

Figure 21: Laminated curved panel: equilibrium paths for $[0]_6$ with C^1-2x2GP and C^2-S_0^3(right) elements.

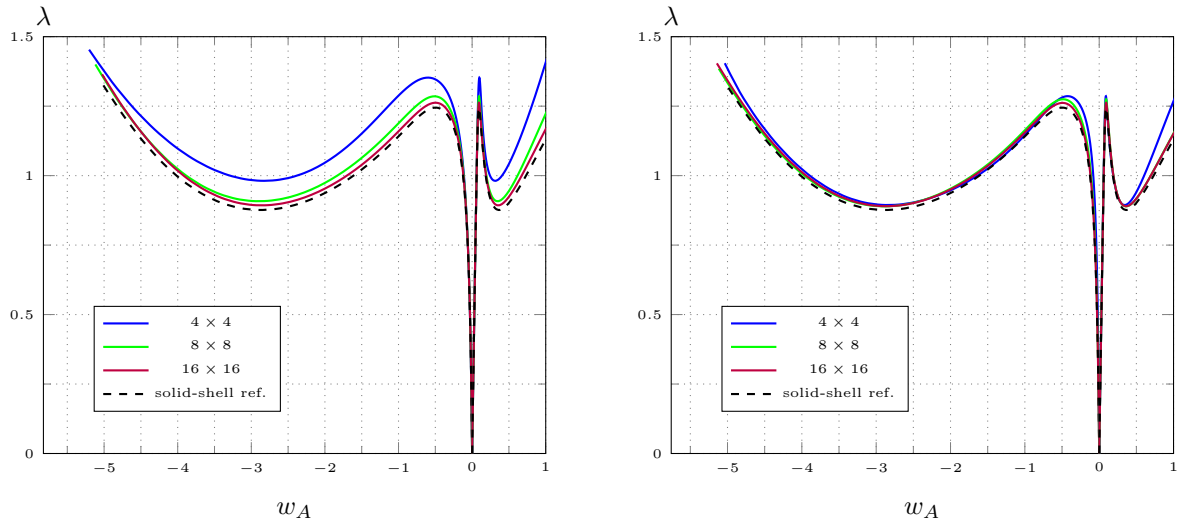

Figure 22: Laminated curved panel: equilibrium paths for $[45/-45/0]_s$ with C^1-2x2GP (left) and C^2-S_0^3 elements (right)

.

E_{11}	$E_{22} = E_{33}$	$\nu_{12} = \nu_{13} = \nu_{23}$	$G_{12} = G_{13} = G_{23}$
2068.50	517.125	0.3	759.58

Table 8: Composite shallow roof: material properties.

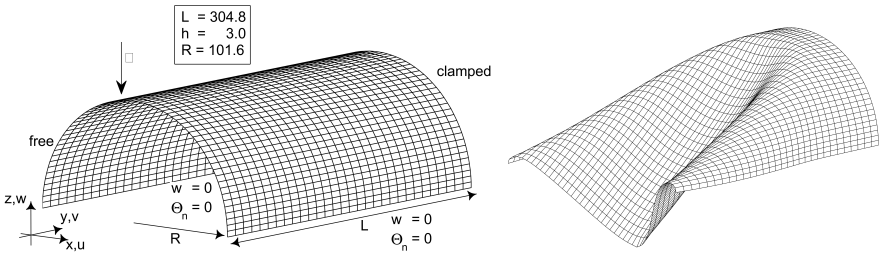

Figure 23: Clamped semi-cylinder: geometry and deformed configuration at the last evaluated equilibrium point for [90/0/90] .

4.5. Clamped semi-cylinder

In Fig. 23, the geometry and the boundary conditions of another classical benchmark [1, 2] are reported. This benchmark is suitable to compare the effectiveness of the proposed model in terms of computational efficiency. The structure is a semi-cylinder loaded by a concentrated force in the middle of one of the curved edges, while the other one is clamped. The vertical displacement of the straight edges is constrained. Due to its symmetry, only onne half of the structure is analyzed. Two cases are considered: an isotropic material, characterized by $E = 2068.50$ and $\nu = 0.3$, and a composite multi-layered material. The local reference system, used for defining the multi-layered material properties, has the direction 1 aligned with the y of the global system while the direction 3 is the normal to the surface from inside out. The stacking sequences of the laminated material are [90/0/90] and [0/90/0], measured with respect to the direction 1 of the local reference system. The material properties are given in Tab.8.

In Fig. 24 the equilibrium paths obtained using the C^1-$2 \times 2GP$ and C^2-S_0^3 elements with the simplified and the exact model are compared. A uniform mesh of 30×30 elements is used in both cases.

Again it is possible to observe that both the simplified and the exact Kirchhoff-Love models furnish the same solutions also for large displacements.

In Fig. 25 some components of the stress field are reported. The results are in agreement with those obtained using the locking-free solid-shell finite element reported in [2].

It is worth noting that the mean time cost of each iteration for the simplified Kirchhoff-Love model is, for this test and with our `MATLAB` implementation, about 22% lower than the cost of the exact one due to the simpler expressions of the tangent matrix and internal force vector.

5. Conclusions

This paper focuses on an efficient formulation of the Kirchhoff-Love model for elastic shells undergoing large deformations in the context of isogeometric analysis. In particular, two main novelty aspects have been addressed: i) the shell model itself, which has been reformulated according to some features of the physical problem, and ii) its efficient and accurate isogeometric implementation. Concerning the first point, a simplified strain measure has been derived by exploiting the hypothesis of small membrane strains. It consists in a simple third order polynomial function of the displacement variables. This leads to a significant simplification of the strain energy derivatives and a consequent reduction of the computational burden for the evaluation of the discrete operators. Since membrane strains are actually very small in bending-dominated thin shell problems, no difference is observed in the numerical results of the standard and of the simplified Kirchhoff-Love shell models, even for very large displacements and for composite materials. The second point of the paper is an isogeometric implementation of the model which does not suffer from interpolation locking

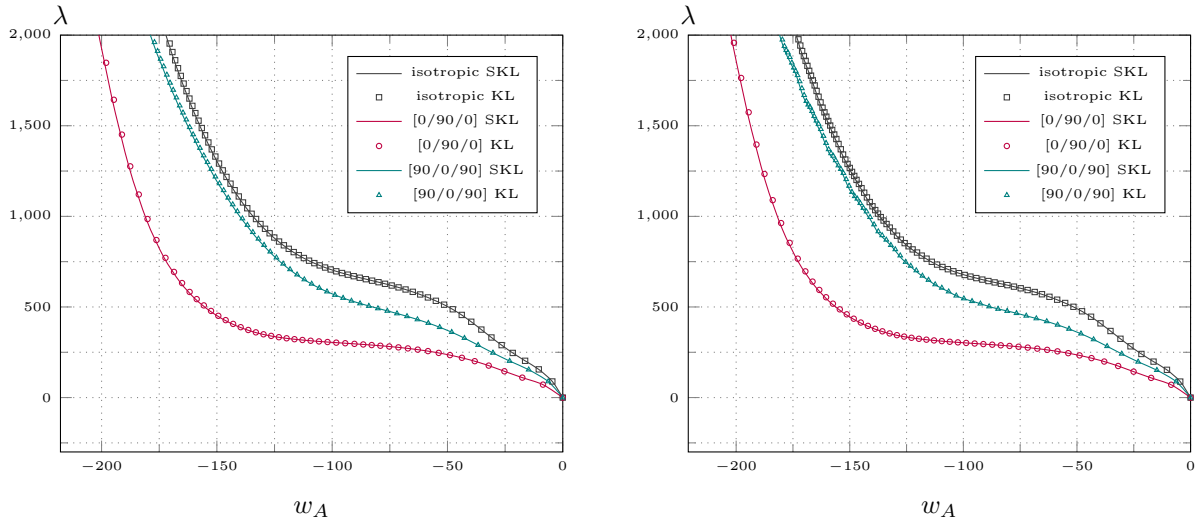

Figure 24: Clamped semi-cylinder: equilibrium paths with element C^1-2x2QP on the left and C^2-S_0^3 on the right, for 30x30 mesh

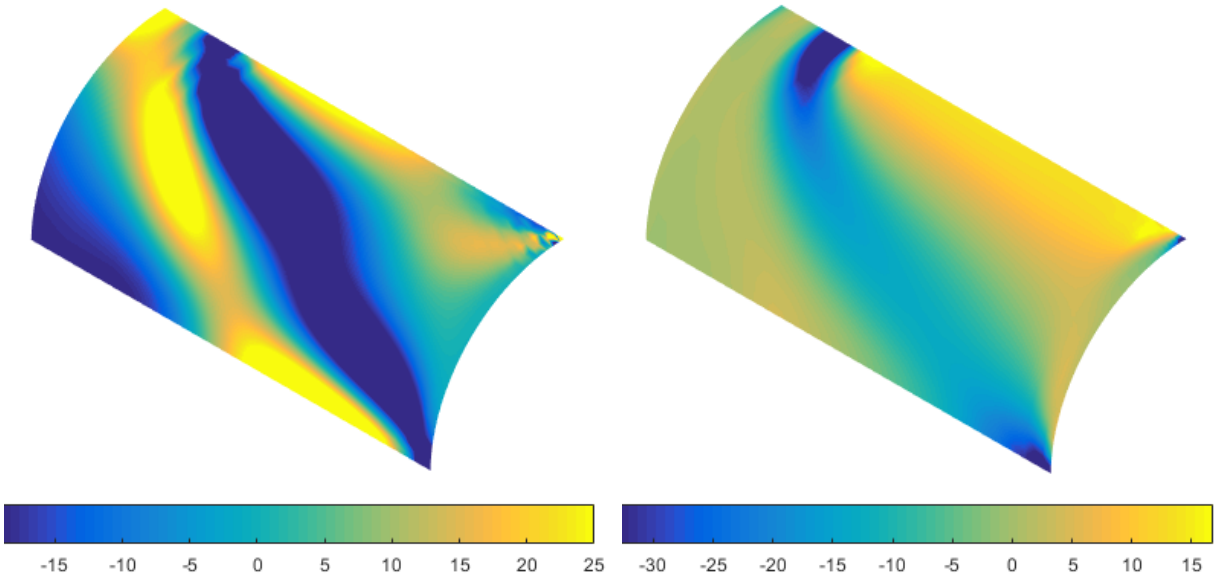

(a) $\mathcal{N}_1$ (b) $\mathcal{M}_1$

Figure 25: Clamped semi-cylinder: stress field at the last evaluated equilibrium point for [90/0/90] .

in the standard displacement-based weak formulation. In geometrically linear problems the Kirchhoff-Love shell model exhibits membrane locking for curved geometries while it is locking free for flat ones. When moving to the large deformation case, the use of a nonlinear strain measure introduces a locking effect also for initially flat structures due to the different interpolation order of the strain contributions. To avoid this locking problem, a numerical investigation on the use of patch-wise reduced integration rules has been carried out for second order C^1 and third order C^2 NURBS. An optimal solution has been identified, consisting of the use of C^2 NURBS with the so-called S_0^3 integration space. This rule allows the use of very coarse meshes, since it avoids the locking issue also for very slender structures, and requires a low number of integration points (about 2.25 per element). Many interesting numerical tests have been carried out, always showing results in very good agreement with the reference solutions, also for laminated engineering structures.

Appendix A. Strain variations for the curvature of the reduced model

The components of the curvature have been defined in Eq.(11). It can be rewritten as

$$\bar{\chi}_{ij} = \frac{1}{\|\mathbf{G}_1 \times \mathbf{G}_2\|} \left(\boldsymbol{g}_{i,j}^T \, \mathbf{W}[\boldsymbol{g}_1]\boldsymbol{g}_2 - \mathbf{G}_{i,j}^T \, \mathbf{W}[\mathbf{G}_1]\mathbf{G}_2) \right) \quad i,j = 1,2 \tag{31}$$

by introducing the spin matrix $\mathbf{W}[\boldsymbol{g}_1]$ associated to vector $\boldsymbol{g}_1$, so that $\mathbf{W}[\boldsymbol{g}_1]\mathbf{a} = \boldsymbol{g}_1 \times \mathbf{a}$ for each vector $\mathbf{a}$.

Given 3 vectors $\mathbf{a}, \mathbf{b}, \mathbf{c}$ the following properties hold

$$\mathbf{a}^T\mathbf{W}[\mathbf{b}]\mathbf{c} = \mathbf{b}^T\mathbf{W}[\mathbf{c}]\mathbf{a} = \mathbf{c}^T\mathbf{W}[\mathbf{a}]\mathbf{b} = -\mathbf{b}^T\mathbf{W}[\mathbf{a}]\mathbf{c} = -\mathbf{c}^T\mathbf{W}[\mathbf{b}]\mathbf{a} = \cdots$$

The first variation of $\bar{\chi}_{ij}$ is then

$$\delta\bar{\chi}_{ij} = \frac{1}{\|\mathbf{G}_1 \times \mathbf{G}_2\|} \left(\boldsymbol{g}_1^T\mathbf{W}[\boldsymbol{g}_2]\delta\mathbf{u}_{,ij} + \boldsymbol{g}_2^T\mathbf{W}[\boldsymbol{g}_{i,j}]\delta\mathbf{u}_{,1} + \boldsymbol{g}_{i,j}^T\mathbf{W}[\boldsymbol{g}_1]\delta\mathbf{u}_{,2} \right)$$

where, we use the following identities

$$\delta\boldsymbol{g}_{i,j} = \delta\mathbf{u}_{,ij} \quad \delta\boldsymbol{g}_1 = \delta\mathbf{u}_{,1} \quad \delta\boldsymbol{g}_2 = \delta\mathbf{u}_{,2}$$

Similarly, the second variation of $\bar{\chi}_{ij}$ is

$$\begin{aligned} \delta\dot{\bar{\chi}}_{ij} = \frac{1}{\|\mathbf{G}_1 \times \mathbf{G}_2\|} \Big\{ & \left(\dot{\mathbf{u}}_{,1}^T \, \mathbf{W}[\boldsymbol{g}_2] - \dot{\mathbf{u}}_{,2}^T \, \mathbf{W}[\boldsymbol{g}_1] \right) \delta\mathbf{u}_{,ij} + \left(\dot{\mathbf{u}}_{,2}^T \, \mathbf{W}[\boldsymbol{g}_{i,j}] - \dot{\mathbf{u}}_{,ij}^T \, \mathbf{W}[\boldsymbol{g}_2] \right) \delta\mathbf{u}_{,1} \\ & + \left(\dot{\mathbf{u}}_{,ij}^T \, \mathbf{W}[\boldsymbol{g}_1] - \dot{\mathbf{u}}_{,1}^T \, \mathbf{W}[\boldsymbol{g}_{i,j}] \right) \delta\mathbf{u}_{,2} \Big\} \end{aligned}$$

Remembering the interpolation in Eq.(12) we have

$$\delta\mathbf{u}_{,i} = \mathbf{N}[\xi,\eta]_{,i} \, \delta\mathbf{d}_e \quad \dot{\mathbf{u}}_{,i} = \mathbf{N}[\xi,\eta]_{,i} \, \dot{\mathbf{d}}_e \quad \delta\mathbf{u}_{,ij} = \mathbf{N}[\xi,\eta]_{,ij} \, \delta\mathbf{d}_e \quad \dot{\mathbf{u}}_{,ij} = \mathbf{N}[\xi,\eta]_{,ij} \, \dot{\mathbf{d}}_e$$

which furnishes the curvature components and their variations as functions of the discrete parameters to be used for the evaluation of the internal force vector in Eq.(25) and the tangent stiffness matrix in Eq.(28).

References

[1] K. Sze, W. Chan, T. Pian, An eight-node hybrid-stress solid-shell element for geometric non-linear analysis of elastic shells, International Journal for Numerical Methods in Engineering 55 (7) (2002) 853–878. doi:10.1002/nme.535.

[2] L. Leonetti, F. Liguori, D. Magisano, G. Garcea, An efficient isogeometric solid-shell formulation for geometrically nonlinear analysis of elastic shells, Computer Methods in Applied Mechanics and Engineering 331 (2018) 159 – 183. doi:https://doi.org/10.1016/j.cma.2017.11.025.
URL `http://www.sciencedirect.com/science/article/pii/S0045782517307429`

[3] J. A. Cottrell, T. J. R. Hughes, Y. Bazilevs, Isogeometric Analysis: Toward Integration of CAD and FEA, 2009. doi:978-0-470-74873-2.

[4] V. P. Nguyen, C. Anitescu, S. P. Bordas, T. Rabczuk, Isogeometric analysis: An overview and computer implementation aspects, Mathematics and Computers in Simulation 117 (2015) 89 – 116. doi:https://doi.org/10.1016/j.matcom.2015.05.008.
[5] K. A. Johannessen, Optimal quadrature for univariate and tensor product splines, Computer Methods in Applied Mechanics and Engineering 316 (2017) 84 – 99, special Issue on Isogeometric Analysis: Progress and Challenges. doi:http://doi.org/10.1016/j.cma.2016.04.030.
[6] C. Adam, T. Hughes, S. Bouabdallah, M. Zarroug, H. Maitournam, Selective and reduced numerical integrations for NURBS-based isogeometric analysis, Computer Methods in Applied Mechanics and Engineering 284 (2015) 732–761. doi:10.1016/j.cma.2014.11.001.
[7] F. Fahrendorf, L. D. Lorenzis, H. Gomez, Reduced integration at superconvergent points in isogeometric analysis, Computer Methods in Applied Mechanics and Engineering 328 (2018) 390 – 410. doi:https://doi.org/10.1016/j.cma.2017.08.028.
URL http://www.sciencedirect.com/science/article/pii/S0045782517303717
[8] G. Sangalli, M. Tani, Matrix-free weighted quadrature for a computationally efficient isogeometric k-method, Computer Methods in Applied Mechanics and Engineering 338 (2018) 117 – 133. doi:https://doi.org/10.1016/j.cma.2018.04.029.
URL http://www.sciencedirect.com/science/article/pii/S0045782518302081
[9] G. Garcea, L. Leonetti, D. Magisano, R. Gonçalves, D. Camotim, Deformation modes for the post-critical analysis of thin-walled compressed members by a Koiter semi-analytic approach, International Journal of Solids and Structures 110-111 (2017) 367–384. doi:10.1016/j.ijsolstr.2016.09.010.
[10] G. Garcea, F. S. Liguori, L. Leonetti, D. Magisano, A. Madeo, Accurate and efficient a posteriori account of geometrical imperfections in Koiter finite element analysis, International Journal for Numerical Methods in Engineering 112 (9) (2017) 1154–1174, nme.5550. doi:10.1002/nme.5550.
[11] D. J. Benson, Y. Bazilevs, M.-C. Hsu, T. J. R. Hughes, Isogeometric shell analysis: The Reissner–Mindlin shell 199 (2010) 276–289.
[12] R. Echter, B. Oesterle, M. Bischoff, A hierarchic family of isogeometric shell finite elements, Computer Methods in Applied Mechanics and Engineering 254 (2013) 170–180. doi:10.1016/j.cma.2012.10.018.
[13] S. Bieber, B. Oesterle, E. Ramm, M. Bischoff, A variational method to avoid locking—independent of the discretization scheme, International Journal for Numerical Methods in Engineering 114 (8) 801–827. arXiv:https://onlinelibrary.wiley.com/doi/pdf/10.1002/nme.5766, doi:10.1002/nme.5766.
URL https://onlinelibrary.wiley.com/doi/abs/10.1002/nme.5766
[14] W. Dornisch, S. Klinkel, B. Simeon, Isogeometric Reissner-Mindlin shell analysis with exactly calculated director vectors, Computer Methods in Applied Mechanics and Engineering 253 (2013) 491–504.
[15] J. Caseiro, R. Valente, A. Reali, J. Kiendl, F. Auricchio, R. Alves de Sousa, Assumed natural strain NURBS-based solid-shell element for the analysis of large deformation elasto-plastic thin-shell structures, Computer Methods in Applied Mechanics and Engineering 284 (2015) 861–880. doi:10.1016/j.cma.2014.10.037.
[16] S. Hosseini, J. J. C. Remmers, C. V. Verhoosel, R. de Borst, An isogeometric solid-like shell element for nonlinear analysis, International Journal for Numerical Methods in Engineering 95 (3) (2013) 238–256. doi:10.1002/nme.4505.
URL http://dx.doi.org/10.1002/nme.4505
[17] R. Bouclier, T. Elguedj, A. Combescure, Efficient isogeometric NURBS-based solid-shell elements: Mixed formulation and B-method, Computer Methods in Applied Mechanics and Engineering 267 (2013) 86–110. doi:10.1016/j.cma.2013.08.002.
[18] J. Kiendl, K.-U. Bletzinger, J. Linhard, R. Wüchner, Isogeometric shell analysis with kirchhoff–love elements, Computer Methods in Applied Mechanics and Engineering 198 (49) (2009) 3902 – 3914. doi:https://doi.org/10.1016/j.cma.2009.08.013.
URL http://www.sciencedirect.com/science/article/pii/S0045782509002680
[19] J. Kiendl, M.-C. Hsu, M. Wu, A. Reali, Isogeometric Kirchhoff–Love shell formulations for general hyperelastic materials, Computer Methods in Applied Mechanics and Engineering 291 (2015) 280–303.
[20] M. Ambati, J. Kiendl, L. De Lorenzis, Isogeometric Kirchhoff–Love shell formulation for elasto-plasticity, Computer Methods in Applied Mechanics and Engineering 340 (2018) 320–339.
[21] A. Buganza Tepole, H. Kabaria, K.-U. Bletzinger, E. Kuhl, Isogeometric Kirchhoff–Love shell formulations for biological membranes, Computer Methods in Applied Mechanics and Engineering 293 (2015) 328–347.
[22] T. Duong, F. Roohbakhshan, R. Sauer, A new rotation-free isogeometric thin shell formulation and a corresponding continuity constraint for patch boundaries, Computer Methods in Applied Mechanics and Engineering 316 (2017) 43–83.
[23] B. Oesterle, R. Sachse, E. Ramm, M. Bischoff, Hierarchic isogeometric large rotation shell elements including linearized transverse shear parametrization, Computer Methods in Applied Mechanics and Engineering 321 (2017) 383 – 405. doi:https://doi.org/10.1016/j.cma.2017.03.031.
URL http://www.sciencedirect.com/science/article/pii/S0045782517302323
[24] A. D. Lanzo, G. Garcea, Koiter's analysis of thin-walled structures by a finite element approach, International Journal for Numerical Methods in Engineering 39 (17) (1996) 3007–3031.
[25] A. D. Lanzo, G. Garcea, R. Casciaro, Asymptotic post-buckling analysis of rectangular plates by HC finite elements, International Journal for Numerical Methods in Engineering 38 (14) (1995) 2325–2345.
[26] F. Cirak, M. Ortiz, Fully C1-conforming subdivision elements for finite deformation thin-shell analysis, International Journal for Numerical Methods in Engineering 51 (2001) 813–833.
[27] L. Greco, M. Cuomo, L. Contrafatto, A reconstructed local $\bar{B}$ formulation for isogeometric kirchhoff–love shells, Computer Methods in Applied Mechanics and Engineering 332 (2018) 462 – 487. doi:https://doi.org/10.1016/j.cma.2018.01.005.
URL http://www.sciencedirect.com/science/article/pii/S0045782518300070
[28] R. Bouclier, T. Elguedj, A. Combescure, An isogeometric locking-free NURBS-based solid-shell element for geometrically nonlinear analysis, International Journal for Numerical Methods in Engineering 101 (10) (2015) 774–808.

doi:10.1002/nme.4834.
[29] L. Leonetti, D. Magisano, F. Liguori, G. Garcea, An isogeometric formulation of the koiter's theory for buckling and initial post-buckling analysis of composite shells, Computer Methods in Applied Mechanics and Engineering 337 (2018) 387 – 410. doi:https://doi.org/10.1016/j.cma.2018.03.037.
URL http://www.sciencedirect.com/science/article/pii/S0045782518301610
[30] J. Kiendl, Y. Bazilevs, M.-C. Hsu, R. Wüchner, K.-U. Bletzinger, The bending strip method for isogeometric analysis of kirchhoff–love shell structures comprised of multiple patches, Computer Methods in Applied Mechanics and Engineering 199 (37) (2010) 2403 – 2416. doi:https://doi.org/10.1016/j.cma.2010.03.029.
URL http://www.sciencedirect.com/science/article/pii/S0045782510001064
[31] A. Goyal, B. Simeon, On penalty-free formulations for multipatch isogeometric kirchhoff–love shells, Mathematics and Computers in Simulation 136 (2017) 78–103.
[32] L. Coox, F. Greco, O. Atak, D. Vandepitte, W. Desmet, A robust patch coupling method for NURBS-based isogeometric analysis of non-conforming multipatch surfaces, Computer Methods in Applied Mechanics and Engineering 316 (2017) 235–260.
[33] A. J. Herrema, E. L. Johnson, D. Proserpio, M. C. H. Wu, J. Kiendl, M.-C. Hsu, Penalty coupling of non-matching isogeometric Kirchhoff-Love shell patches with application to composite wind turbine blades, Comput. Methods Appl. Mech. Engrg. (2018) in press.
[34] D. Magisano, L. Leonetti, G. Garcea, Advantages of the mixed format in geometrically nonlinear analysis of beams and shells using solid finite elements, International Journal for Numerical Methods in Engineering 109 (9) (2017) 1237–1262. doi:10.1002/nme.5322.
[35] G. Garcea, G. Trunfio, R. Casciaro, Mixed formulation and locking in path-following nonlinear analysis, Computer Methods in Applied Mechanics and Engineering 165 (1-4) (1998) 247–272.
[36] D. Magisano, L. Leonetti, G. Garcea, How to improve efficiency and robustness of the Newton method in geometrically non-linear structural problem discretized via displacement-based finite elements, Computer Methods in Applied Mechanics and Engineering 313 (2017) 986 – 1005. doi:http://dx.doi.org/10.1016/j.cma.2016.10.023.
[37] F. Maurin, F. Greco, W. Desmet, Isogeometric analysis for nonlinear planar pantographic lattice: discrete and continuum models, Continuum Mechanics and Thermodynamicsdoi:10.1007/s00161-018-0641-y.
URL https://doi.org/10.1007/s00161-018-0641-y
[38] F. Maurin, F. Greco, S. Dedoncker, W. Desmet, Isogeometric analysis for nonlinear planar kirchhoff rods: Weighted residual formulation and collocation of the strong form, Computer Methods in Applied Mechanics and Engineering 340 (2018) 1023 – 1043. doi:https://doi.org/10.1016/j.cma.2018.05.025.
URL http://www.sciencedirect.com/science/article/pii/S0045782518302706
[39] W. T. Les Piegl, The NURBS book, 1997. doi:10.1007/978-3-642-59223-2.
[40] G. Garcea, A. Madeo, R. Casciaro, The implicit corotational method and its use in the derivation of nonlinear structural models for beams and plates, J. Mech. Mater. Struct. 7 (6) (2012) 509–539. doi:10.2140/jomms.2012.7.509.
[41] C. H. Thai, H. Nguyen-Xuan, S. P. A. Bordas, N. Nguyen-Thanh, T. Rabczuk, Isogeometric Analysis of Laminated Composite Plates Using the Higher-Order Shear Deformation Theory, Mechanics of Advanced Materials and Structures 22 (6) (2015) 451–469. doi:10.1080/15376494.2013.779050.
[42] Y. Guo, M. Ruess, A layerwise isogeometric approach for NURBS-derived laminate composite shells, Composite Structures 124 (2015) 300 – 309. doi:https://doi.org/10.1016/j.compstruct.2015.01.012.
[43] J.-E. Dufour, P. Antolin, G. Sangalli, F. Auricchio, A. Reali, A cost-effective isogeometric approach for composite plates based on a stress recovery procedure, Composites Part B: Engineering 138 (2018) 12 – 18. doi:https://doi.org/10.1016/j.compositesb.2017.11.026.
URL http://www.sciencedirect.com/science/article/pii/S1359836817320383
[44] E. Riks, An incremental approach to the solution of snapping and buckling problems, International Journal of Solids and Structures 15 (7) (1979) 529–551. doi:10.1016/0020-7683(79)90081-7.
[45] F. S. Liguori, A. Madeo, D. Magisano, L. Leonetti, G. Garcea, Post-buckling optimisation strategy of imperfection sensitive composite shells using koiter method and monte carlo simulation, Composite Structures 192 (2018) 654 – 670. doi:https://doi.org/10.1016/j.compstruct.2018.03.023.
URL http://www.sciencedirect.com/science/article/pii/S0263822317339776